

Stony Brook University



OFFICIAL COPY

The official electronic file of this thesis or dissertation is maintained by the University Libraries on behalf of The Graduate School at Stony Brook University.

© All Rights Reserved by Author.

Amyloid Accelerators: Small Molecules that Accelerate Amyloid Formation by Amylin

A Thesis Presented

by

Yuan Chen

to

The Graduate School

in Partial Fulfillment of the

Requirements

for the Degree of

Master of Science

in

Chemistry

Stony Brook University

May 2014

Stony Brook University

The Graduate School

Yuan Chen

We, the thesis committee for the above candidate for the
Master of Science degree, hereby recommend
acceptance of this thesis.

**Daniel P. Raleigh – Thesis Advisor
Professor, Department of Chemistry**

**Scott Laughlin – Second Reader
Assistant Professor, Department of Chemistry**

**David F. Green – Third Reader
Associate Professor, Department of Applied Mathematics and Statistics**

This thesis is accepted by the Graduate School

Charles Taber
Dean of the Graduate School

Abstract of the Thesis

Amyloid Accelerators: Small Molecules that Accelerate Amyloid Formation by Amylin

by

Yuan Chen

Master of Science

in

Chemistry

Stony Brook University

2014

Amyloid formation *in vivo* plays a role in the pathology of more than 25 diseases. Amyloid formation by Islet Amyloid Polypeptide (IAPP) in the pancreas is a pathophysiological feature of type-2 diabetes. Much work has been performed in order to unravel the mechanisms of IAPP amyloid formation *in vitro* and recent studies suggest that toxic oligomers are generated during the formation of amyloids. Thus, it may be useful to look for compounds that accelerate fibril formation and reduce the lifetime of toxic intermediates. (S)-(+)-Flurbiprofen has been previously proven to accelerate IAPP amyloid formation. Computational simulation suggested the N-terminus of IAPP plays an important role in the interaction. In order to further understand the mechanism, the effect of (S)-(+)-Flurbiprofen were tested with different mutants of IAPP. The results suggest that the overall charge of IAPP is important in the interaction between negatively charged (S)-(+)-Flurbiprofen and positively charged IAPP. Moreover, a new compound, 4-[(4-chlorophenyl) thio] thiophene-3-carboxylic acid was identified and shown to accelerate amyloid formation by IAPP.

Table of Contents

List of Figures.....	vi
List of Abbreviations	viii
Acknowledgments	ix
1. Introduction.....	1
1.1 Islet Amyloid Polypeptide (IAPP).....	1
1.2 IAPP Amyloid Formation.....	2
1.3 Inhibition of IAPP Amyloid Formation	3
1.4 IAPP Amyloid Structure	3
1.5 (S)-(+)-Flurbiprofen Accelerates IAPP Amyloid Formation	4
2. Analyzing the Role of N-terminus in Interaction of (S)-(+)-Flurbiprofen with IAPP.....	14
2.1 Identification of Interaction between Wild Type IAPP and (S)-(+)-Flurbiprofen.....	14
2.2 Materials and Methods	14
2.2.1 Docking.....	14
2.2.2 Peptide Synthesis	15
2.2.3 Sample Preparation.....	16
2.2.4 Thioflavin-T Assays.....	16
2.2.5 Transmission Electron Microscopy (TEM).....	17
2.3 Results and Discussion	17
2.3.1 Docking Results	17

2.3.2 (S)-(+)-Flurbiprofen Accelerates Amyloid Formation by Wild Type IAPP, 8-37 IAPP, Acetylated-8-37 IAPP and C2S C7S IAPP.....	18
2.3.3 Acetylated-8-37 IAPP Appears to Be the Least Sensitive to the Effect of (S)-(+)-Flurbiprofen	19
2.4 Conclusions	20
3. Discovery of a New Compound that Accelerates IAPP Amloid Formation	31
3.1 Finding New Compounds through DUD-E.....	31
3.2 Materials and Methods.....	32
3.2.1 Peptide Synthesis	32
3.2.2 Sample Preparation.....	33
3.2.3 Thioflavin-T Assays.....	34
3.2.4 UV Spectrum.....	35
3.2.5 Transmission Electron Microscopy (TEM).....	35
3.2.6 ¹ H NMR	35
3.2.7 Preparation of Vesicles.....	36
3.3 Results and Discussion	36
3.3.1 4-[(4-chlorophenyl) thio] thiophene-3-carboxylic acid (Compound A) Accelerates Amyloid Formation by Wild Type IAPP, But the Other Compounds Have No Effect	36
3.3.2 Compound A Does Not Aggregate	37
3.4 Conclusions	38
Appendix.....	47
References.....	80

List of Figures

- Figure 1-1. Primary sequence of IAPP from different species.
- Figure 1-2. Formation of mature IAPP.
- Figure 1-3. Structure of resveratrol and EGCG.
- Figure 1-4. IAPP fibril structure, due to Eisenberg and coworker.
- Figure 1-5. IAPP fibril structure, due to Tycko and coworker
- Figure 1-6. Experimentally proved compounds that accelerate IAPP amyloid formation.
- Figure 1-7. Comparison of TEM images of wild type IAPP alone and with a 20-fold excess of (S)-(+)-Flurbiprofen.
- Figure 1-8. A typical Thioflavin-T assay.
- Figure 2-1. The IAPP fibril structure used for docking.
- Figure 2-2. Docking results for (S)-(+)-Flurbiprofen with the IAPP fibril model.
- Figure 2-3. Foot Print Score for the first 20 residues of wild type IAPP.
- Figure 2-4. Primary sequences of wild type IAPP, 8-37 IAPP, acetylated-8-37 IAPP, C2S C7S IAPP.
- Figure 2-5. Kinetic curves and TEM images of wild type IAPP with and without (S)-(+)-Flurbiprofen.
- Figure 2-6. Kinetic curves and TEM images of 8-37 IAPP with and without (S)-(+)-Flurbiprofen.
- Figure 2-7. Kinetic curves and TEM images of C2S C7S IAPP with and without (S)-(+)-Flurbiprofen.
- Figure 2-8. Kinetic curves and TEM images of acetylated-8-37 IAPP with and without

(S)-(+)-Flurbiprofen.

- Figure 2-9. Comparison of wild type IAPP (black), 8-37 IAPP (red), C2S C7S IAPP (green), acetylated-8-37 IAPP (yellow) at five concentrations.
- Figure 3-1. Decoys generated from DUD-E (<http://decoys.docking.org>) and purchased from Sigma-Aldrich.
- Figure 3-2. Primary sequences of wild type human IAPP and the IAPP mutant I26P.
- Figure 3-3. Thioflavin-T curves of wild type IAPP compared to that of same peptide with 20-fold excess of 4-[(4-chlorophenyl) thio] thiophene-3-carboxylic acid.
- Figure 3-4. UV scan of compound A from 700 nm to 200 nm.
- Figure 3-5. Kinetic curves and TEM images of wild type IAPP and 4-[(4-chlorophenyl) thio] thiophene-3-carboxylic acid.
- Figure 3-6. T50 value comparison.
- Figure 3-7. NMR spectrum of 4-[(4-chlorophenyl) thio] thiophene-3-carboxylic acid.
- Figure 3-8. Structure of DOPG and kinetic curves of I26P-IAPP in the presence and absence of DOPG.
- Figure 4-1. Kinetic curves of wild type IAPP with and without 4-(2,4-dimethylphenyl)-2,2,3-trimethylcyclopentanecarboxylic acid.
- Figure 4-2. Kinetic curves of wild type IAPP with and without alpha-(3-Chloro-6-Methylphenylimino)-P-Cresol.
- Figure 4-3. Kinetic curves of wild type IAPP with and without 2-(2-Hydroxyphenyl) benzothiazole.

List of Abbreviations

DIPEA	N,N-Diisopropylethylamine
DMF	N,N-Dimethylformamide
DMSO	dimethyl sulfoxide
DOPG	1,2-dioleoyl- <i>sn</i> -glycero-3-phospho-(1'- <i>rac</i> -glycerol)
DUD	directory of useful decoys
DUD-E	directory of useful decoys, enhanced
HFIP	hexafluoroisopropanol
HOBt	1-Hydroxybenzotriazole
Fmoc	9-Fluorenylmethoxycarbonyl
IAPP	islet amyloid polypeptide
TEM	transmission electron microscopy
Tris	2-amino-2-hydroxymethyl-propane-1,3-diol
NMR	nuclear magnetic resonance
RP-HPLC	reverse phase high performance liquid chromatography
(S)-(+)-Flurbiprofen	(S)-(+)-2-fluoro- α -methyl-4-biphenylacetic acid
T50	time point when 50% final intensity is reached during a thioflavin-T assay
UV	ultraviolet

Acknowledgments

I would like to express my gratitude to Prof. Raleigh first. Thank him for providing me the opportunity to work in his lab. I really like this project because I can work on what I was interested in since my undergraduate study as well as learning new knowledge. I found myself enjoy working on peptides and proteins and really hope that I can pursue further in this area. His brilliant ideas always inspire me. I have learned a lot in this lab.

I thank Prof. Laughlin and Prof. Green for being my committee members and giving me valuable comments on my thesis.

Thanks to all the group members: Rehana Arter, Bowu Luan, Ivan Peran, Zachary Ridgway, Natalie Stenzosk, Ling-Hsien Tu, Hui Wang, Matthew Watson, Amy Wong and Xiaoxue Zhang. I would like to express my gratitude especially for Ling-Hsien Tu. She basically taught me everything in lab and experiments. I would also like to thank Harris Noor, who did a lot of work and made the discovery of the small compound.

Finally, I want to thank my families back in China. Without their love and support, I would not have finished my study here.

1. Introduction

1.1 Islet Amyloid Polypeptide (IAPP)

Improperly folded proteins or polypeptides naturally present in the human body can change their proper configuration forming insoluble amyloid fibrils in which β -strands run perpendicular to the long axis of the fibril. Amyloid fibrils share several common features including similar cross β -sheet structure, affinity for dye binding and birefringence after staining [1]. They contribute to many human diseases including Huntington's disease, Parkinson's disease and type-2 diabetes [2].

Pancreatic islet amyloid deposits are a pathophysiological feature of type-2 diabetes [3], which was first reported in 1900s [4]. However, it was not until 1987 that a 37-residue polypeptide hormone, which was named amylin or islet amyloid polypeptide (IAPP), was shown to be the protein component of islet amyloid [5, 6]. Normally, IAPP is soluble and natively unfolded as a monomer, but it can form amyloid in type-2 diabetes [5-7]. IAPP is found in all mammals and believed to play important roles in gastric emptying control, glucose homeostasis and suppression of glucagon release [7]. The study of IAPP plays an important role in diabetes therapy development. A large amount of work has been put in the research of IAPP amyloid formation control.

Mature human IAPP is a 37-residue long polypeptide. It has a positively charged N-terminus and an amidated C-terminus. It has three positive charges at pH 7.4 and a Cys 2 - Cys 7 disulfide bridge. The propensity to form amyloid is related to the sequence of IAPP [8]. Primary sequences from different species are shown in Figure 1-1. Human IAPP forms amyloid fibrils while rat/mouse IAPP not. The primary sequence of rat/mouse has 6 different residues from

human IAPP. The segment between residues 23 and 27 is crucial to amyloid formation [9]. The Pro substitutions at positions 25, 28 and 29 may lead to steric hindrance and contribute to rat/mouse IAPP inability to form amyloid [3].

1.2 IAPP Amyloid Formation

IAPP is originally synthesized as an 89 residue long pre-proform [10]. After processing in the Golgi and insulin secretory granule, IAPP is released with insulin [7]. The process is shown in Figure 1-2. It remains unclear whether the initial aggregation is intracellular or extracellular. The process of IAPP fibril formation can induce β -cell apoptosis and dysfunction [11]. One proposed mechanism of IAPP toxicity indicates that IAPP oligomers are able to induce membrane leakage [12]. There is a close relationship between the ability of IAPP to induce membrane leakage and lipid composition in biophysics studies. Kinetic studies with toxic wild type IAPP and nontoxic IAPP mutants suggest that they can all induce membrane leakage without the presence of β -sheet or α -helical structure [13]. Compared to rat IAPP, which does not form amyloid fibrils, the fibril growth of human IAPP promotes additional leakage. IAPP-mediated membrane damage is sensitive to the substitutions at His-18.

Bachanan and colleagues identified an oligomeric intermediate formed during the lag phase with parallel β -sheet [14]. They used 2D infrared spectroscopy and isotope labeling to monitor the fibril formation kinetics. Their experiments and simulations showed that the hydrophobic region FGAIL (hIAPP 23-27) was crucial to the aggregation process. FGAIL forms a transient β -sheet intermediate on pathway. A free energy barrier of FGAIL from β -sheet to disordered loop drives the formation of amyloid. The experiments were done at a high peptide concentration. The situation may be different at a lower concentration.

1.3 Inhibition of IAPP Amyloid Formation

Several compounds have been proven to be able to inhibit the amyloid formation induced by IAPP. Resveratrol (Figure 1-3 A) found in red wine can inhibit IAPP fibril formation as well as lipid induced fibril formation [15]. Dynamic simulation studies suggest that resveratrol hinders stacking of aromatic rings and blocks the lateral growth of a single-layered β -sheet oligomer [16]. EGCG (Figure 1-3 B) can effectively interact with monomers, intermediates and amyloids. EGCG is thought to function by diverting amyloidogenic proteins into off-pathway non-toxic aggregates. The compound is able to remodels IAPP amyloid fiber but not reverse amyloid formation. A study of analogues of EGCG showed that none of aromatic residues, interactions with amino groups or sulfhydryls is required in the interaction. It was shown that the gallate ester and the trihydroxyl phenyl ring effect the inhibition ability of EGCG [17].

1.4 IAPP Amyloid Structure

Since crystallization of full length IAPP has not been successfully achieved, the structure of IAPP fibrils is not yet fully illustrated. But there are two models based on same experimental data: one is derived from X-ray studies and the other from solid state NMR of small peptides. The existing fibril models share several common features. Each IAPP molecule adopts a hairpin structure containing two β -strands with a bend-loop. Two columns of symmetry monomers pack together as a basic unit [3]. IAPP fibrils are made up of extended β -sheet structure running perpendicular to the fibril axis [18]. Wiltzius and his colleagues [9] have crystallized two segments of IAPP, which were residues 21-27 NNFGAIL and 28-33 SSTNVG. They considered the segment between residues 28 to 33 to be crucial to fibril formation. Along with structural data they built an atomic-based fibril model. The model is shown in Figure 1-4. Two human IAPP molecules form a steric zipper around the fibril axis. The segment NNFGAIL starts from a

hairpin turn to steric zipper interface, followed by the segment of SSTNVG in the central extension. The fibril grows perpendicular with a left-handed twist of 3.4 Å per layer. The model adopts a rigid packing pattern and the overall diameter is 64 Å.

Another model proposed by Tycko's group [19] was based on measurements of scanning transmission electron microscopy and solid-state nuclear magnetic resonance (NMR), shown in Figure 1-5. The basic unit contains four layers of parallel β -sheet. The β -strands contain residues 8-17 and 28-37. The bend loop is from residue 18 to 27.

1.5 (S)-(+)-Flurbiprofen Accelerates IAPP Amyloid Formation

The study of IAPP is often compared to A β amyloid formation, which is believed to be an important cause for Alzheimer's disease [20]. According to studies of patients with long-term use of non-steroidal anti-inflammatory drugs (NSAIDs), they have a lower risk of developing Alzheimer's disease [21]. But the effects of NSAIDs on IAPP have not been studied. Harris Noor, a former graduate student in the Raleigh group, made the discovery that flurbiprofen (mixtures of (R)-Flurbiprofen and (S)-(+)-Flurbiprofen), an NSAIDs, can accelerate IAPP fibril formation and reduce toxicity [22]. Later other compounds with similar structures have proven to have the ability to accelerate IAPP fibril formation (Figure 1-6). (S)-(+)-Flurbiprofen was chosen for further study. Cytotoxicity assays conducted by Dr. Abedini at NYU Medical School showed that (S)-(+)-Flurbiprofen is not toxic to cells even at a very high concentration. She also showed that (S)-(+)-Flurbiprofen protects β -cells against the toxic effects of IAPP [22]. The hypothesis made by the Raleigh group is that the fibril itself is not toxic, but the intermediates appearing during the progress of amyloid formation are toxic. Flurbiprofen can accelerate amyloid formation, which reduces lifetime of toxic intermediates and protects β -cells.

(S)-(+)-Flurbiprofen shortens the lag phase of wild type IAPP without changing the morphology of the fibril (Figure 1-8). Increasing the concentration of (S)-(+)-Flurbiprofen causes the lag phase of IAPP to shorten and the final fluorescence to be higher. Usually higher fluorescence intensity indicates that more fibrils have formed. However, there is no experiment that confirms, (S)-(+)-Flurbiprofen induces more fibrils.

Aggregation of some small compounds can lead to micelle-like structures that can bind amyloidogenic proteins [23]. Negatively charged micelles can accelerate amyloid formation by positively charged human IAPP. But control experiments conducted by former group members shows that this is not the case. It still remains unknown how (S)-(+)-Flurbiprofen interacts with IAPP.

This thesis is based on the finding that (S)-(+)-Flurbiprofen is able to accelerate fibril formation of IAPP. A computational simulation was conducted between wild type IAPP and (S)-(+)-Flurbiprofen in order to possibly illustrate the interaction mechanism. Experimental studies using IAPP mutants were conducted to examine factors that influence the interaction with (S)-(+)-Flurbiprofen. These used thioflavin-T assays to follow amyloid formation. Thioflavin-T does not interact with soluble IAPP monomer. But it binds to fibril and has UV fluorescence. A typical thioflavin-T assay curve is shown in Figure 1-9. Usually it is divided into 3 parts, which is the lag phase, the growth phase and the plateau respectively. By observing the interaction of (S)-(+)-Flurbiprofen with different IAPP segments and mutants, the mechanism was discussed.

Directory of Useful Decoys, Enhanced (DUD-E) was used in this thesis to screen compounds. Decoys are small molecules with similar 1-D physical properties but dissimilar 2-D topology. By providing the structure of (S)-(+)-Flurbiprofen to the online tool (<http://decoys.docking.org>), decoys of it can be generated. Through testing these decoys, a new compound, 4-[(4-chlorophenyl) thio] thiophene-3-carboxylic acid, was found to have similar effect with (S)-(+)-Flurbiprofen.

	1	10	20	30	37
Human CGRP1:	ACDTATCVT	HRLAGLLSRS	GGVVKNNFVP	TNVGSKAF	
Human CGRP2:	ACNTATCVT	HRLAGLLSRS	GGMVKSNFVP	TNVGSKAF	
Human:	KCNTATCAT	QRLANFLVHS	SNNFGAILSS	TNVGSNTY	
Monkey:	KCNTATCAT	QRLANFLVRS	SNNFGTILSS	TNVGSDTY	
Macaque:	KCNTATCAT	QRLANFLVRS	SNNFGTILSS	TNVGSDTY	
Baboon:	ICNTATCAT	QRLANFLVRS	SNNFGTILSS	TNVGSNTY	
Porcine:	KCNMATCAT	QHLANFLDRS	RNNLGTIFSP	TKVGSNTY	
Cow:	KCGTATCET	ORLANFLAPS	SNKLGAI FSP	TKMGSNTY	
Cat:	KCNTATCAT	QRLANFLIRS	SNNLGAILSP	TNVGSNTY	
Dog:	KCNTATCAT	ORLANFLVRT	SNNLGAILSP	TNVGSNTY	
Rat:	KCNTATCAT	QRLANFLVRS	SNNLGPVLPP	TNVGSNTY	
Mouse:	KCNTATCAT	QRLANFLVRS	SNNLGPVLPP	TNVGSNTY	
Guinea Pig:	KCNTATCAT	QRLTNFLVRS	SHNLGAALLP	TDVGSNTY	
Hamster:	KCNTATCAT	QRLANFLVHS	NNNLGPVLS P	TNVGSNTY	
Degu:	KCNTATCAT	QRLTNFLVRS	SHNLGAALPP	TKVGSNTY	
Ferret:	KCNTATCVT	QRLANFLVRS	SNNLGAILLP	TDVGSNTY	
Rabbit:	CNTVTCAT	QRLANFLIHS	SNNFGAFLPP	S	
Hare:		T QRLANFLIHS	SNNFGAFLPP	T	

Figure 1-1. Primary sequence of IAPP from different species. Residues different from human IAPP are highlighted in red. The sequences for rabbit and hare are not complete. IAPP from primates and cats can form amyloid while dogs, rodents and cows do not. Porcine and ferret IAPP are significantly less amyloidogenic than human IAPP. Only partial sequences are available for rabbit and hare IAPP. The figure is adapted from [3].

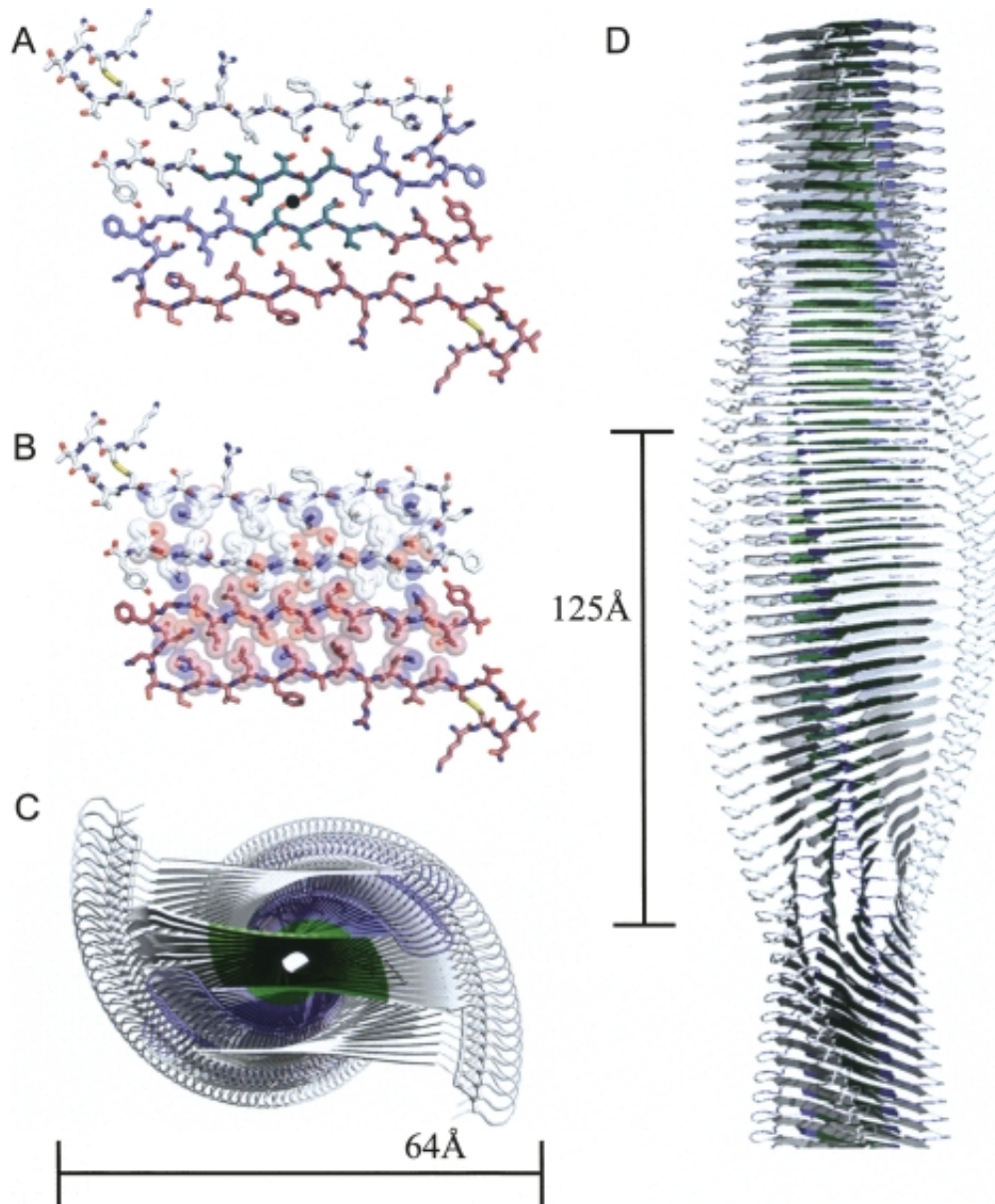


Figure 1-4. IAPP fibril structure, due to Eisenberg and coworker. (A) View down the fibril axis. NNFGAIL, shown in blue, is part of the hairpin turn and the start of the zipper interface. SSTNVG, shown in green, is in the zipper interface. (B) Space-filling representation shows the tight steric zipper interface on two IAPP molecules. (C) View down fibril axis with a diameter of 64 Å. (D) View perpendicular to fibril axis of the same fibril with a length of 125 Å. The figure is adapted from [9].

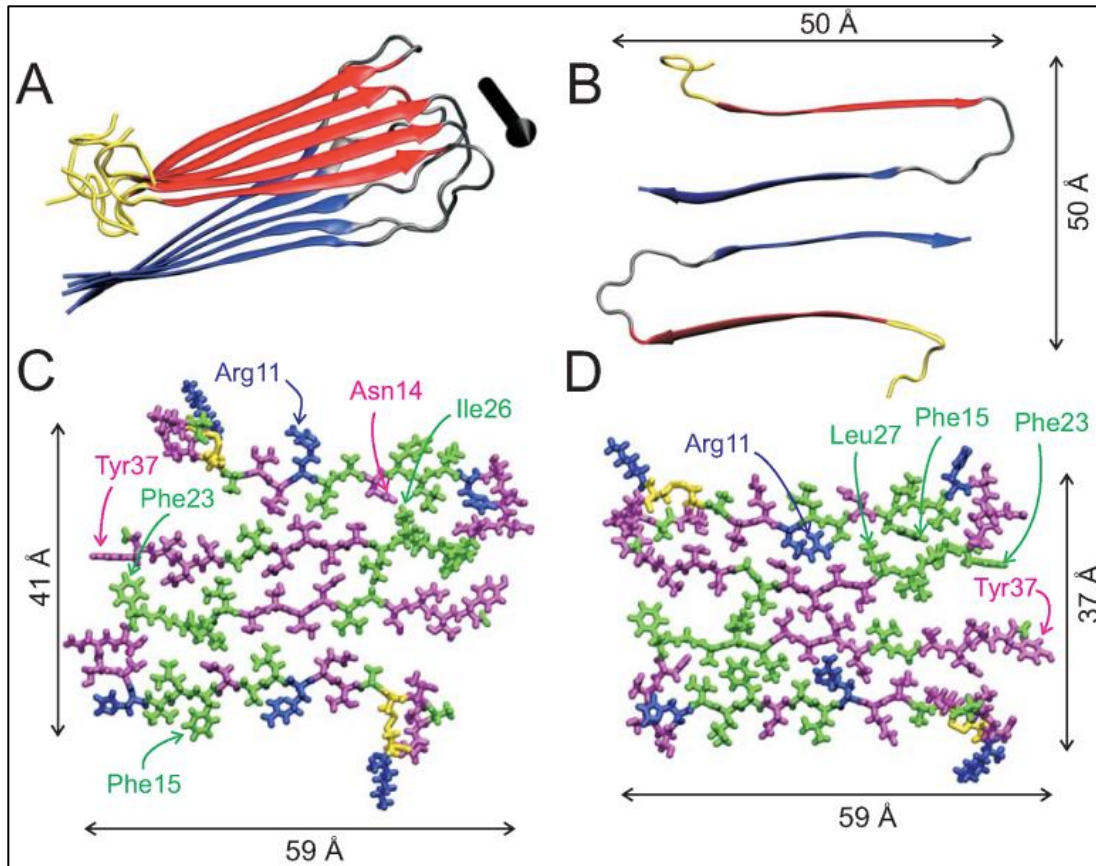


Figure 1-5. IAPP fibril structure, due to Tycko and coworker. (A) One cross- β molecular layer shown as ribbons. The N-terminal β -strand segment is shown in red and the blue is the C-terminal β -strand segment with the black arrow indicating the fibril axis. (B) Two IAPP molecules in the protofilament viewed down from the axis. (C and D) Two possible models are shown in all-atom representations. Colors indicate different charged, hydrophobic or hydrophilic residues. Cys is in yellow. The figure is adapted from [19].

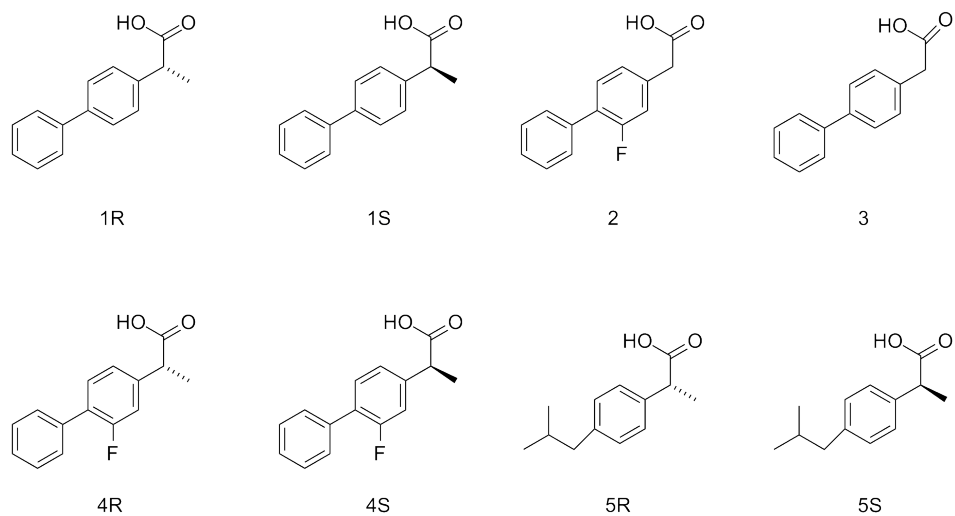


Figure 1-6. Experimentally proved compounds that accelerate IAPP amyloid formation. 1R, (R)-(-)-2-[1,1'-biphenyl]-4-ylpropanoic acid; 1S, (S)-(-)-2-[1,1'-biphenyl]-4-ylpropanoic acid; 2, 2-(2-Fluoro-[1,1'-biphenyl]-4-yl)acetic acid; 3, 4-Biphenylacetic acid; 4R, R-Flurbiprofen; 4S, (S)-(+)-Flurbiprofen; 5R, R-Ibuprofen; 5S, S-Ibuprofen.

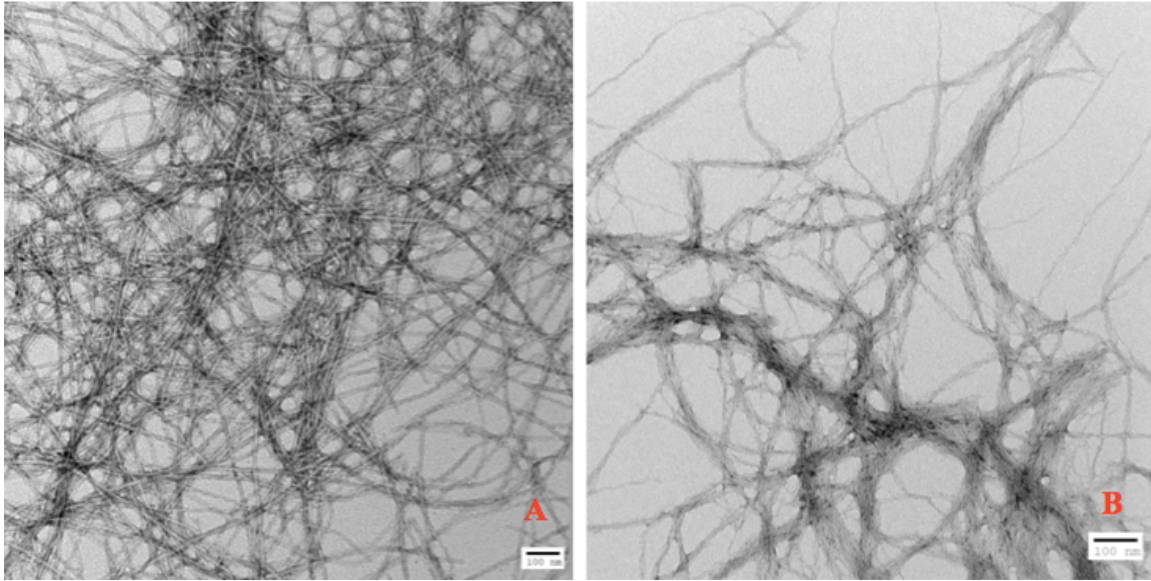
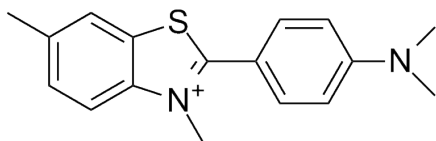
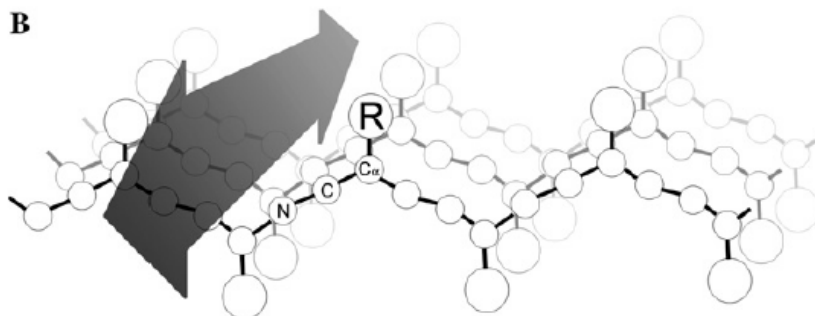


Figure 1-7. Comparison of TEM images of wild type IAPP alone and with a 20-fold excess of (S)-(+)-Flurbiprofen. A. TEM images of wild type IAPP (sample solution contains 0.25% DMSO). B. TEM images of wild type IAPP with 20-fold Flurbiprofen (sample solution contains 0.25% DMSO). (S)-(+)-Flurbiprofen does not change morphology of wild type IAPP. The scale bar is 100 nm. The data was collected by a former group member Harris Noor.

A



B



C

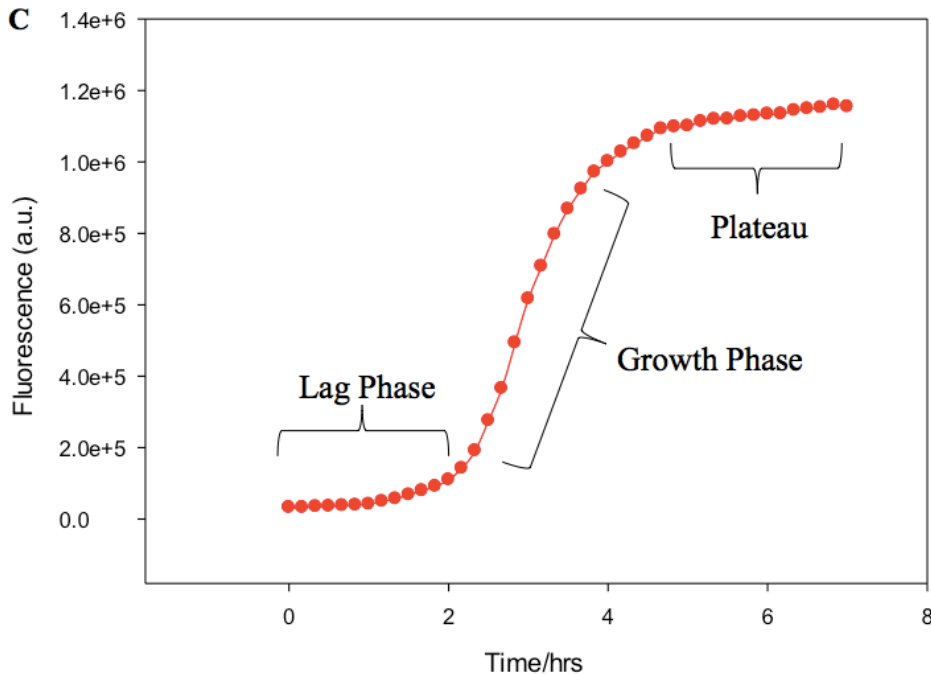


Figure 1-8. A typical Thioflavin-T assay. A. Thioflavin-T structure. B. Binding model of Thioflavin-T within a β -sheet channel formed by surface sidechains. Adapted from [24]. C. Typical sigmoidal curve of a thioflalvin-T assay. Lag phase: no obvious fluorescence detected, indicating no detectable fibrils formed. Growth phase: The rapid growth of intensity shows the formation of fibrils. Plateau: Fibril formation reaches equilibrium.

2. Analyzing the Role of N-terminus in Interaction of (S)-(+)-Flurbiprofen with IAPP

2.1 Identification of Interaction between Wild Type IAPP and (S)-(+)-Flurbiprofen

Dock is a molecular docking program. It consists of two key parts: a search algorithm and a scoring function [25]. The search algorithm samples both the relative orientations between two objects (usually a protein and a small molecule) as well as their conformations. A scoring function ranks these binding models by proposing the top-scoring pose as the global minimum (the lowest binding free energy). Dock 6 (one kind of docking programs) has been used to identify possible binding sites or important residues in the interaction of (S)-(+)-Flurbiprofen with IAPP fibrils. It is important to focus on the point whether (S)-(+)-Flurbiprofen binds to IAPP fibrils. This may shed light on the mechanisms of amyloid formation.

At pH 7.4, an IAPP molecule has 3-unit positive charges, which come from the positively charged N-terminus, Lys-1 and Arg-11. There are two positive charges on the N-terminus. In this thesis, (S)-(+)-Flurbiprofen was tested with different segments of IAPP to analyze the role of the N-terminus in the interaction.

2.2 Materials and Methods

2.2.1 Docking

Dr. Vadim Patsalo, a former graduate student in the Raleigh group, used the Eisenberg model [9] together with MD simulations to build a simulated model for an IAPP fibril. Each IAPP molecule has 3 positive charges: a positively charged N-terminus, Lys-1 and Arg-11. The model (not available in Protein Data Bank) is shown in Figure 2-1. The structure of (S)-(+)-Flurbiprofen was generated by MOE, charges added by Chimera. Docking between the wild type IAPP fibril and (S)-(+)-Flurbiprofen was conducted with Dock 6. The foot print score was also

calculated in order to show the interaction of (S)-(+)-Flurbiprofen with each residue.

2.2.2 Peptide Synthesis

Four IAPP segments and mutants were synthesized. They were wild type IAPP, 8-37 IAPP, acetylated-8-37 IAPP and C2S C7S IAPP (Figure 2-4). All the peptides were synthesized using a CEM microwave peptide synthesizer on 0.1mmol scale with 9-fluorenylmethoxycarbonyl (Fmoc) chemistry. Fmoc-protected pseudoproline (oxazolidine) dipeptide derivatives were used to prevent chemical reactions between amino acid side chains [26]. Solvents were ACS-grade. Fmoc- Polyethylene glycol- polystyrene (Fmoc-PAL-PEG-PS) resin was used to provide an amidated C-terminus. Standard Fmoc reaction cycles were used. The first residue attached to the resin; the pseudoproline dipeptide derivatives, all β -branched residues and all residues directly following a β -branched residue were double coupled. For acetylated-8-37 IAPP, an acetylation step after synthesis was needed. 5 mM acetic anhydride, 0.2 ml DIPEA and 0.027g HOBt were dissolved in 10 ml DMF as the acetylation solution. Peptides were cleaved from the resin using standard TFA (trifluoroacetic acid) method. Crude peptides were dissolved in 20% (by volume) acetic acid and lyophilized before oxidation. Then, peptides were oxidized in dimethyl sulfoxide (DMSO) at room temperature [27].

Purification was done via reverse-phase high-performance liquid chromatography (RP-HPLC) with a Higgins C18 preparative column. Analytical HPLC was used to follow the oxidation process. The buffer system consists of buffer A (100% H₂O and 0.045% HCl, by volume) and buffer B (80% acetonitrile, 20% H₂O and 0.045%HCl, by volume). 10% - 60% buffer B in 60 minutes was used for the purification of acetylated-8-37 IAPP. The peak of acetylated-8-37 appeared from 45 minutes. 20%-60% buffer B in 40 minutes was used for the purification of the other three kinds of peptides. The peaks of wild type IAPP, 8-37 IAPP and

C2S C7S IAPP appeared from 28 minutes, 26 minutes and 28 minutes respectively.

The masses of pure peptides were confirmed by matrix-assisted laser desorption/ionization time-of-flight mass spectrometry (MALDI-TOF MS): wild type IAPP, 3903.3 (expected) and 3903.6 (observed); 8-37 IAPP, 3183.5 (expected) and 3183.0 (observed); acetylated-8-37 IAPP, 3225.5 (expected) and 3225.2 (observed); C2S C7S IAPP, 3873.2 (expected) and 3874.4(observed).

2.2.3 Sample Preparation

Peptide stock solutions were prepared in 100% hexafluoroisopropanol (HFIP) at 1.6mM and filtered through a 0.20 μm syringe filter. All stock solutions were stored at $-20\text{ }^{\circ}\text{C}$. The peptide solution was measured into an eppendorf tube and lyophilized for at least 20 hours. The final concentration of IAPP in sample solution was 16 μM .

(S)-(+)-Flurbiprofen was purchased from Santa Cruz Biotechnology (sc-205503A). It was dissolved in dimethyl sulfoxide (DMSO) at 128 mM and diluted to 64 mM, 32 mM and 6.4 mM. The final concentration of (S)-(+)-Flurbiprofen was 320 μM , 160 μM , 80 μM , 16 μM respectively. In the experiment the final concentration of DMSO was 1.25%.

2.2.4 Thioflavin-T Assays

The thioflavin-T assays were performed on a Beckman model D880 plate reader. The excitation filter was 430 nm and emission filter was 485 nm. The experiments were performed in a Corning 96-well plate at $25\text{ }^{\circ}\text{C}$, which was sealed with Corning sealing tape to minimize evaporation.

All the peptides were prepared in hexafluoroisopropanol (HFIP) to a final concentration of 1.6 mM. The HFIP stock solution was filtered through a 0.20 μm syringe filter to remove seeds.

Aliquots of filtered stock solution were distributed into eppendorf tubes and lyophilized. Considering the poor solubility of acetylated-8-37 IAPP in buffer, all the dry peptides were dissolved in DMSO before adding Tris-HCl (20 mM, pH 7.4) buffer. The DMSO concentration in experiments with acetylated-8-37 is the same as with others. 120 μ l of 32 mM thioflavin-T solution was added before measurements. For experiments with (S)-(+)-Flurbiprofen, stock solutions in different concentrations were diluted into the thioflavin-T and peptides solution. For experiments without (S)-(+)-Flurbiprofen, the same amount of DMSO was added to the mixture solution as a control. The final concentration of peptide was 16 μ M. The final concentrations of (S)-(+)-Flurbiprofen were 320 μ M, 160 μ M, 80 μ M, 16 μ M and 0 μ M respectively. Each sample contained 1.25% DMSO (by volume). The data was analyzed using SigmaPlot v12.

2.2.5 Transmission Electron Microscopy (TEM)

TEM images were collected at the Life Science Microscopy Center at Stony Brook University. 15 μ l of the sample from the end of each kinetics study was placed on a carbon-coated 300 mesh copper grid for 1 minute, and then negatively stained with saturated uranyl acetate for 1 minute.

2.3 Results and Discussion

2.3.1 Docking Results

The binding pose with the highest score is shown in Figure 2-2 using a spheres representation. The best score was -42.74 kcal/mol. The binding position of negatively charged (S)-(+)-Flurbiprofen was very close to the positively charged N-terminus of IAPP. The foot print score contains two parts: Van der Waals interactions and electrostatic interactions. The lower the foot print score, the more favorable the binding is. For Van der Waals interactions, the top two

residues were Arg-11 and Lys-1, scored -191.33 kcal/mol and -146.21 kcal/mol respectively. For electrostatic interactions, Arg-11 and residue Lys-1 still ranked top two and the scores were -271.45 kcal/mol and -239.67 kcal/mol respectively. It should be noted that Lys-1 in this case had two positive charges since the N-terminus was contained in the first residue when docking. The foot print scores have been shown in Figure 2-3. They suggest that Lys-1 and Arg-11 are the most important residues in the interaction between (S)-(+)-Flurbiprofen and the IAPP fibril. The docking experiment indicated a favorable electrostatic interaction between IAPP fibrils and (S)-(+)-Flurbiprofen.

2.3.2 (S)-(+)-Flurbiprofen Accelerates Amyloid Formation by Wild Type IAPP, 8-37 IAPP, Acetylated-8-37 IAPP and C2S C7S IAPP

The sequences of wild type IAPP, 8-37 IAPP, acetylated-8-37 IAPP and C2S C7S IAPP are shown in Figure 2-4. 8-37 IAPP is a partial segment of wild type IAPP. It has a charged N-terminus but not a positively charged Lys. Overall it has two positive charges. It lacks Cys-2 and Cys-7 so there is no disulfide bridge. Acetylated-8-37 IAPP shares the same features with 8-37 IAPP, but its N-terminus is acetylated. The overall charge of acetylated-8-37 is +1. C2S C7S IAPP has three positive charges. Cys-2 and Cys-7 were mutated to Ser, which are similar in size, so there is no disulfide bridge formed in this peptide.

The thioflavin-T monitored curves of IAPP in different concentrations of (S)-(+)-Flurbiprofen are shown in Figure 2-5 A. The lag phase of wild type IAPP prepared in DMSO is 17 hours. This is longer than peptide without DMSO. (S)-(+)-Flurbiprofen has little effect on wild type IAPP amyloid formation at 16 μ M (1:1 ratio of wild type IAPP and (S)-(+)-Flurbiprofen). At 80 μ M (1:5 ratio of wild type IAPP and (S)-(+)-Flurbiprofen), (S)-(+)-Flurbiprofen exhibits the ability to accelerate amyloid formation. 160 μ M (1:10) and 320 μ M

(1:20) were tested at the same time. The higher the concentration of (S)-(+)-Flurbiprofen, the more obvious the effect is. The kinetics confirms that (S)-(+)-Flurbiprofen can accelerate fibril formation while increase the fluorescence intensity. The results agree with those of experiments performed earlier by Harris Noor, Ping Cao and Ling-Hsien Tu. Usually higher intensity indicates that more fibrils have formed. But it is unknown whether the amount of fibrils has increased. TEM images (Figure 2-5 B) showed that there is no significant change in morphology between wild type IAPP itself and the peptide with 20-fold (S)-(+)-Flurbiprofen.

Compared to wild type IAPP, the lag phase of 8-37 IAPP is much shorter, which is 6 hours. (S)-(+)-Flurbiprofen can shorten the lag phase of 8-37 IAPP while increase the final fluorescence intensity. The effects of (S)-(+)-Flurbiprofen become more obvious at higher concentrations (Figure 2-6 A). The morphology of 8-37 IAPP fibrils and 20-fold (S)-(+)-Flurbiprofen sample is similar to that of wild type IAPP (Figure 2-6 B).

C2S C7S IAPP has similar kinetic features with 8-37 IAPP (Figure 2-7 A). The morphology of C2S C7S IAPP fibrils show a similar structure with wild type IAPP (Figure 2-7 B).

(S)-(+)-Flurbiprofen has a similar effect on the kinetics and morphology of acetylated-8-37 IAPP (Figure 2-8). The lag phase of acetylated-8-37 IAPP is 2 hours, which is the shortest among the four kinds of peptides. The lyophilized peptide has poor solubility in Tris-HCl buffer (20 mM, pH 7.4).

2.3.3 Acetylated-8-37 IAPP Appears to Be the Least Sensitive to the Effect of (S)-(+)-Flurbiprofen

In order to compare the effect of (S)-(+)-Flurbiprofen on different peptides, the value of t50 in each condition was calculated. The t50 value is defined here as the time point when the kinetic curve reaches half of its final intensity during a thioflavin-T assay. The t50 comparison is shown

in Figure 2-9. For each peptide, the t50 value of sample with (S)-(+)-Flurbiprofen was divided by that of the control condition and the data was plotted as normalized t50. At 1:20 ratio of peptide and (S)-(+)-Flurbiprofen, the t50 value of acetylated-8-37 IAPP is 59.2% of the control group. Compared to the same ratio of wild type IAPP (29.7%), 8-37 IAPP (35.5%) and C2S C7S IAPP (40.7%), acetylated-8-37 IAPP is the least sensitive to the effect of (S)-(+)-Flurbiprofen. Acetylated-8-37 IAPP is also the least sensitive at 1:10 ratio of peptide and (S)-(+)-Flurbiprofen. At higher concentrations (ratio 1:10 and 1:20), wild type IAPP is the most sensitive to the effects of (S)-(+)-Flurbiprofen. At lower concentrations (ratio 1:1 and 1:5), (S)-(+)-Flurbiprofen accelerates all the four peptides and the effects were similar.

2.4 Conclusions

There are limitations in the docking process. Currently there is no fully crystalized IAPP fibril structure to use as a target. The IAPP fibril structure used here is based on the Eisenberg model, which is tightly packed. The real fibril structure may adopt a less strictly packed structure that is more similar to the model developed by Tycko and his colleagues. The crystallization of the full-length fibril remains to be a challenge. The results still provide several clues in revealing the mechanism: (S)-(+)-Flurbiprofen binds closely to the N-terminus of IAPP fibril; Lys-1 and Arg-11 are important in binding of (S)-(+)-Flurbiprofen with wild type IAPP in terms of electrostatic interactions and Van der Waals interactions. Thus the kinetic studies between (S)-(+)-Flurbiprofen and wild type IAPP, 8-37 IAPP, acetylated-8-37 IAPP and C2S C7S IAPP were conducted in order to analyze the role of the N-terminus in acceleration of amyloid formation.

The results showed that (S)-(+)-Flurbiprofen was able to accelerate fibril formation for all four peptides without changing the fibril morphology. The kinetic results suggested that disulfide is not very important in the binding of (S)-(+)-Flurbiprofen. Acetylated-8-37 IAPP has only one

positive charge. It appears to be the least sensitive one to the effects of (S)-(+)-Flurbiprofen. However, the lag phase of acetylated-8-37 fibril formation process is 2 hours, which is much shorter than that of wild type (17 hours). The fact that the lag phase of acetylated-8-37 IAPP is so short makes it hard to use this molecule to test if charge interactions are important. Consider a simple possibility: suppose that the lag phase consisted of a fast step and a slow step and imagine that (S)-(+)-Flurbiprofen only affected the slow step. Also suppose that the truncation and acetylation eliminated the slow step. In this example, which may or may not correspond to the reality, (S)-(+)-Flurbiprofen may still interact with the peptide, but, since the slow step had already been eliminated, no significant effects would be observed on the value of t_{50} . According to the results of t_{50} comparison, residues from 1-7 may not be required for (S)-(+)-Flurbiprofen binding but the overall charges are important. The t_{50} comparison of four peptides is not sufficient enough to confirm the effect of (S)-(+)-Flurbiprofen. The fibril formation mechanism of four peptides should be considered.

The mechanism of (S)-(+)-Flurbiprofen binding is still unknown. The fluorescence intensity might imply that more fibrils formed while (S)-(+)-Flurbiprofen accelerated amyloid formation, but the TEM images of samples in the presence of (S)-(+)-Flurbiprofen were similar to those of wild type IAPP in morphology and in quantity. A more quantitative analysis of fibril formation needs to be done in the future. The UV absorbance of (S)-(+)-Flurbiprofen itself does not interfere with thioflavin-T but it is still possible that (S)-(+)-Flurbiprofen changes the binding of thioflavin-T. If so, another assay is needed for further study of (S)-(+)-Flurbiprofen with IAPP peptides.

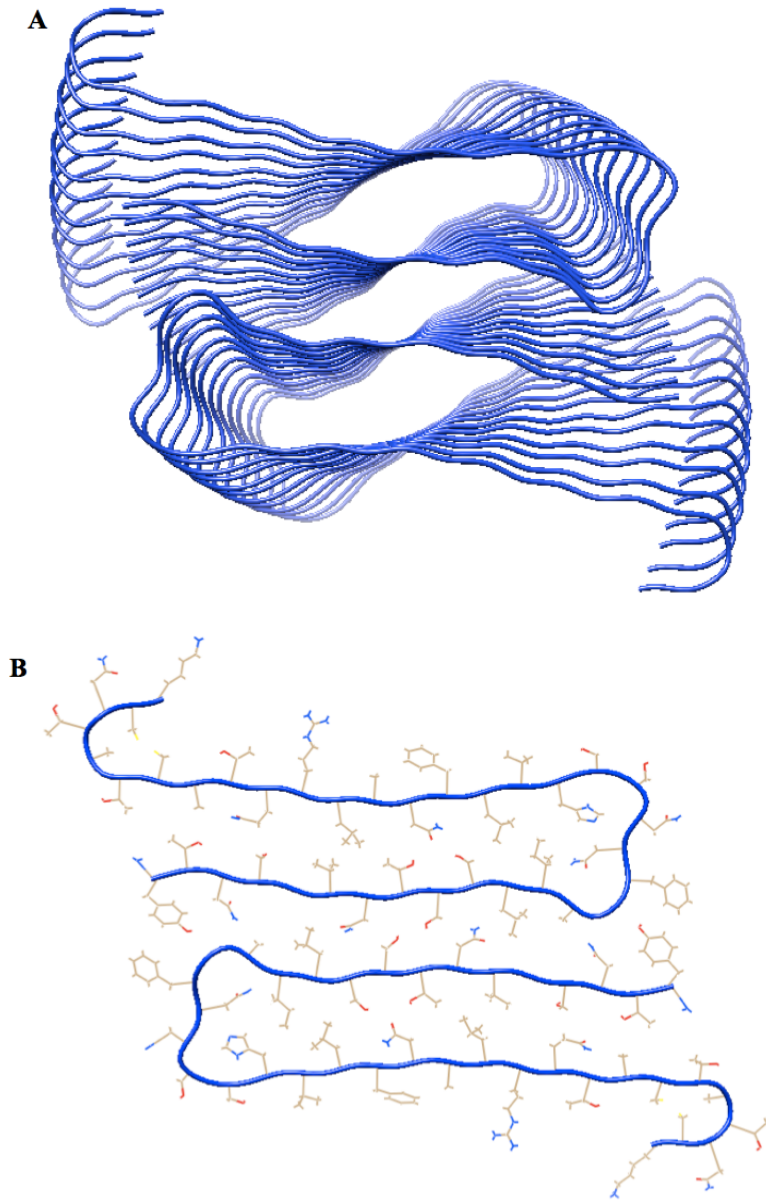


Figure 2-1. The IAPP fibril structure used for docking (View down from the axis). The structure is based on Eisenberg model[9]. A. View of the whole structure. B. One layer of the same structure showing the side chains.

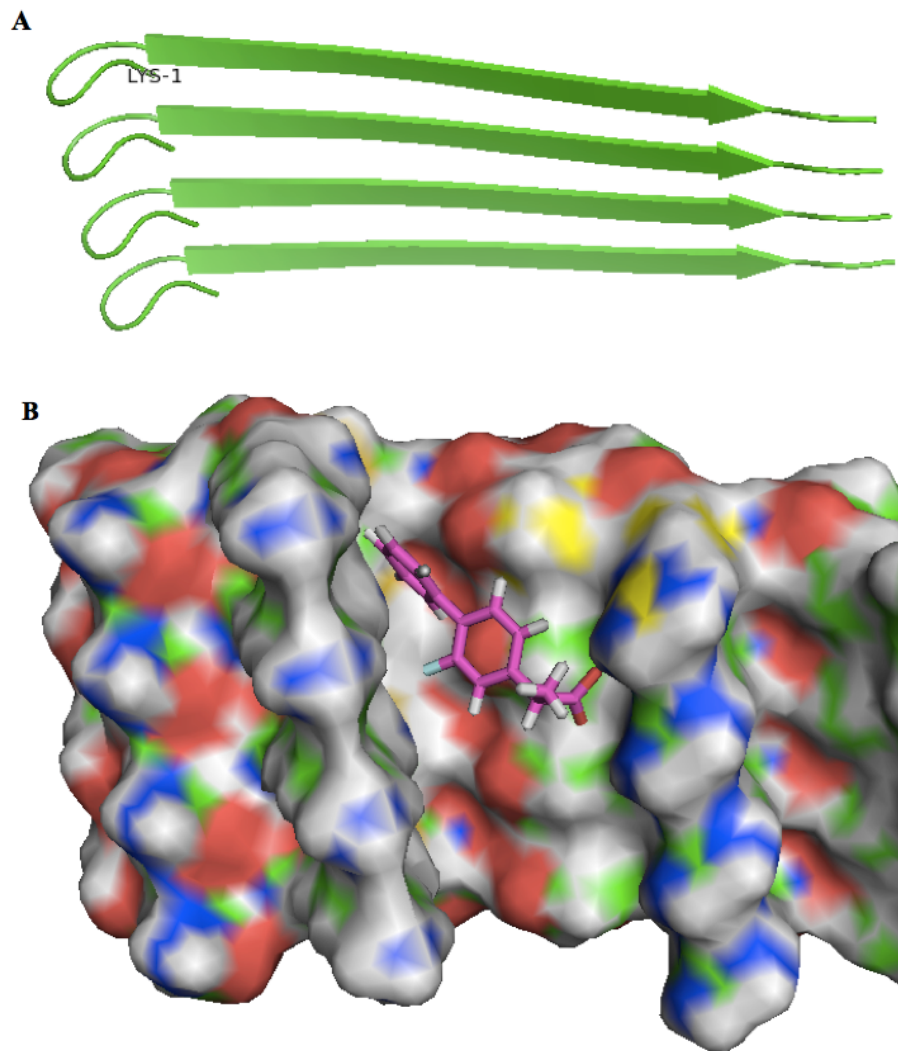


Figure 2-2. Docking results for (S)-(+)-Flurbiprofen with the IAPP fibril model. A. Part of the fibril structure shown in ribbon, consisting of four layers of residues 1 to 20 of IAPP. B. Highest ranking pose. For (S)-(+)-Flurbiprofen, carbons are shown in pink, oxygen in red and fluorine in blue. Fibril structure is shown in sphere. The colors indicate different charges.

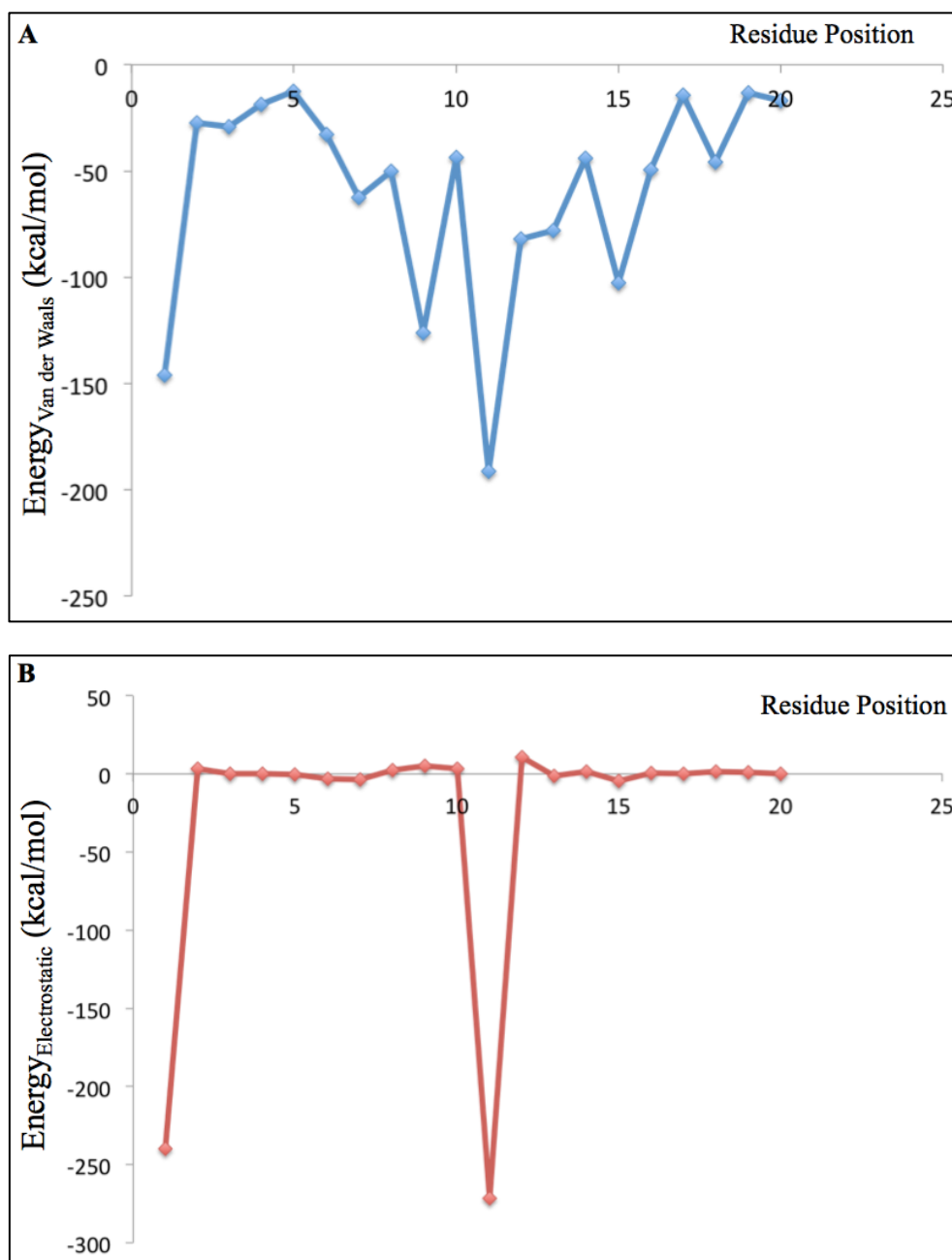


Figure 2-3. Foot Print Score for the first 20 residues of wild type IAPP. It suggests the interaction between each residue and (S)-(+)-Flurbiprofen. Residues after the 20th residue are omitted because there is no significant interaction. A. Foot print score of Van der Waals interaction. The top two residues are Arg-11 and Lys-1, scored -191.33 kcal/mol and -146.21 kcal/mol respectively. B. Foot print score of electrostatic interaction. Arg-11 and Lys-1 still rank top two and the scores are -271.45 kcal/mol and -239.67kcal/mol respectively.

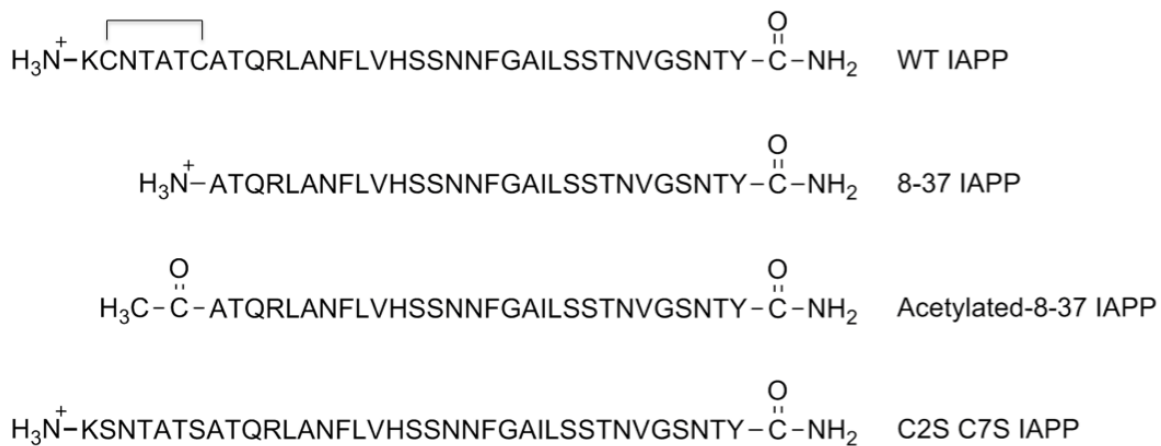


Figure 2-4. Primary sequences of wild type IAPP, 8-37 IAPP, acetylated-8-37 IAPP, C2S C7S IAPP. 8-37 IAPP has a positive charged N-terminus. Acetylated-8-37 IAPP has an acetylated-N-terminus. C2S C7S IAPP shares the same electrostatic features with wild type IAPP, but does not have a disulfide bridge.

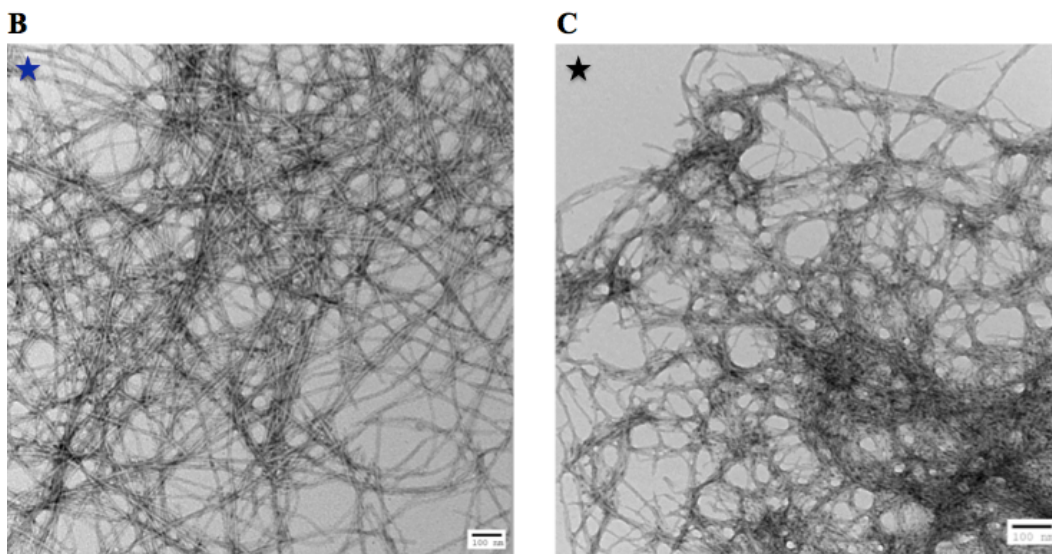
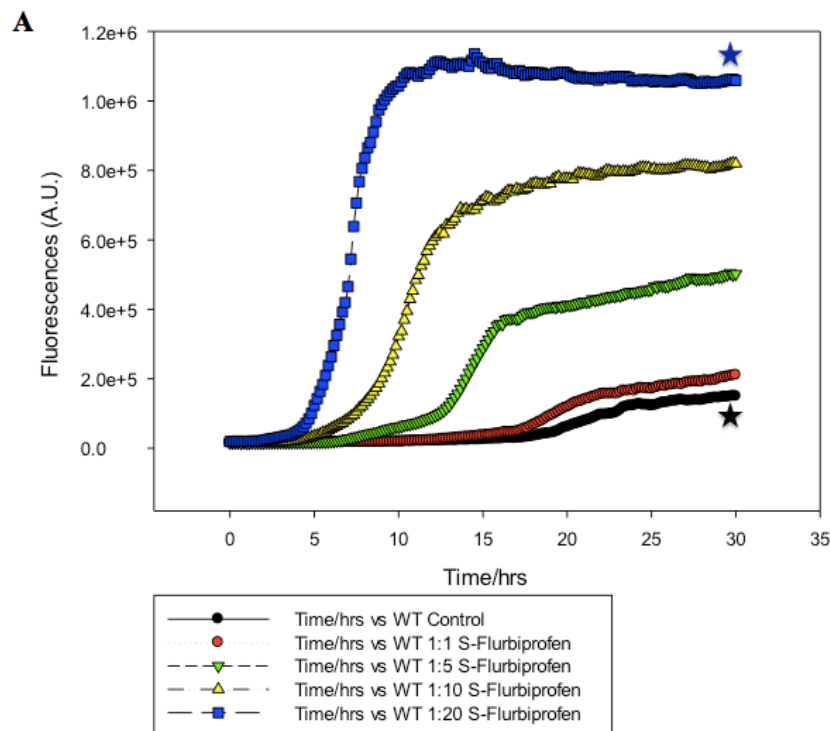


Figure 2-5. Kinetic curves and TEM images of wild type IAPP with and without (S)-(+)-Flurbiprofen. A. Thioflavin-T curves of 16 μ M wild type human IAPP without (S)-(+)-Flurbiprofen (black), 16 μ M wild type human IAPP at ratio 1:1 (red), 1:5 (green), 1:10 (yellow) and 1:20 (blue). Experiments were conducted at 25 $^{\circ}$ C, 20 mM Tris-HCl buffer, pH 7.4, 1.25% DMSO. B. TEM images of wild type IAPP control at the end of kinetic study. C. TEM images of wild type IAPP with 20-fold (S)-(+)-Flurbiprofen at the end of kinetic study. Scale bar is 100 nm.

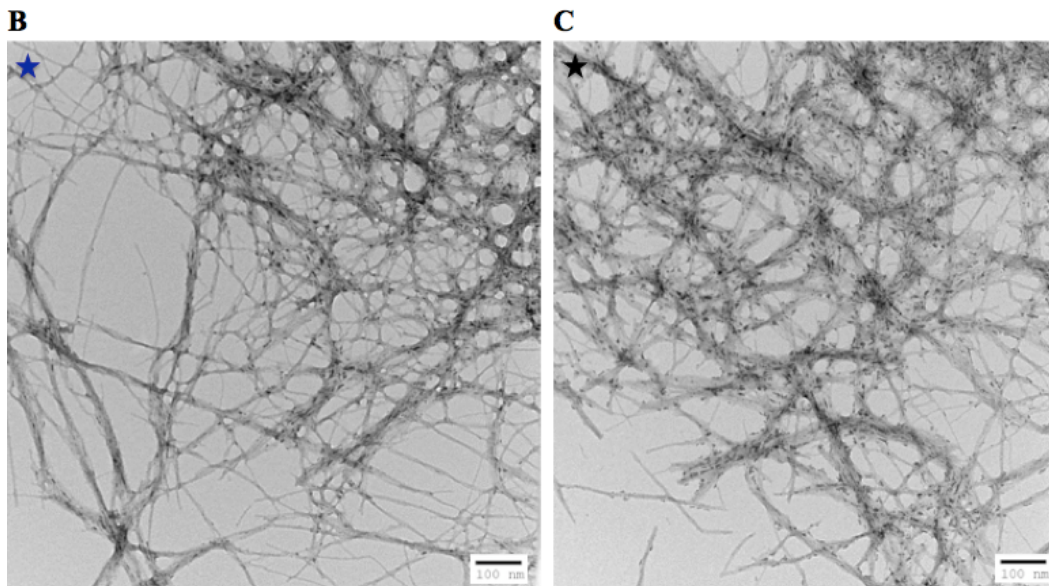
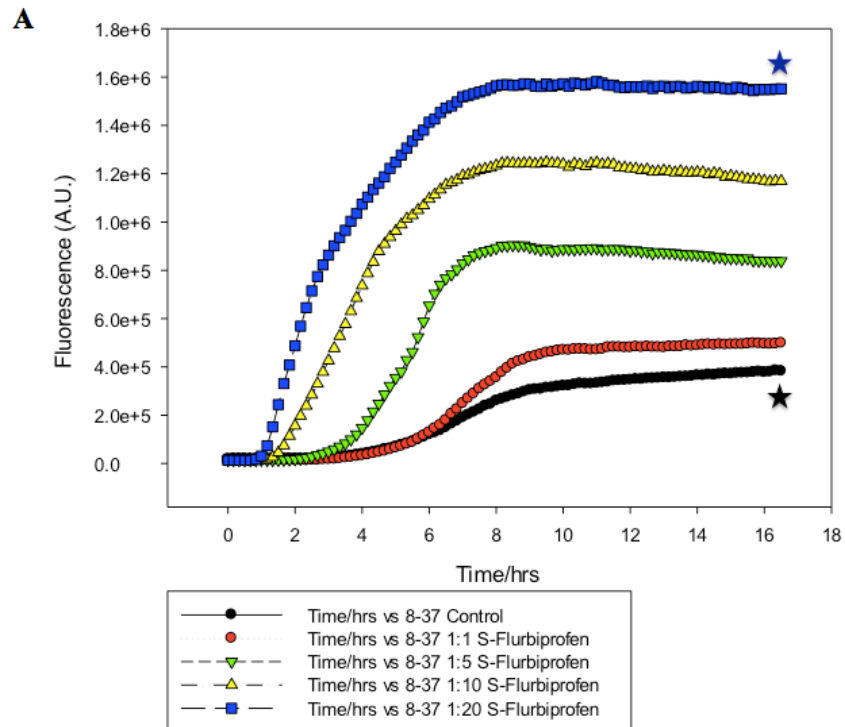


Figure 2-6. Kinetic curves and TEM images of 8-37 IAPP with and without (S)-(+)-Flurbiprofen. A. Thioflavin-T curves of 16 μ M 8-37 IAPP without (S)-(+)-Flurbiprofen (black), 16 μ M 8-37 IAPP at ratio 1:1 (red), 1:5 (green), 1:10 (yellow) and 1:20 (blue). Experiments were conducted at 25 $^{\circ}$ C, 20 mM Tris-HCl buffer, pH 7.4, 1.25% DMSO. B. TEM images of 8-37 IAPP control at the end of kinetic study. C. TEM images of 8-37 IAPP with 20-fold (S)-(+)-Flurbiprofen at the end of kinetic study. Scale bar is 100 nm.

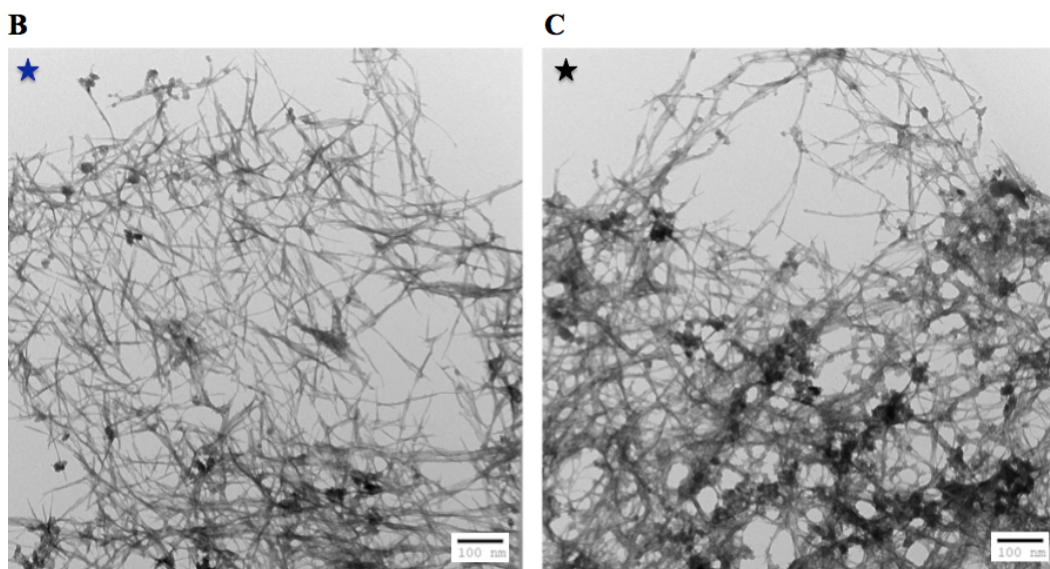
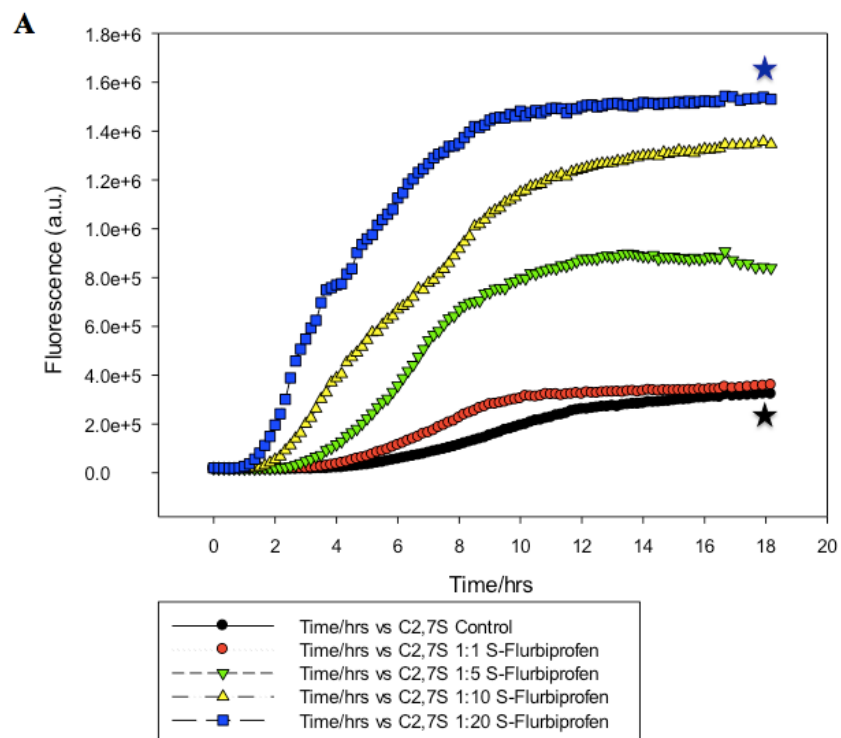


Figure 2-7. Kinetic curves and TEM images of C2S C7S IAPP with and without (S)-(+)-Flurbiprofen. A. Thioflavin-T curves of 16 μ M C2S C7S IAPP without (S)-(+)-Flurbiprofen (black), 16 μ M C2S C7S IAPP at ratio 1:1 (red), 1:5 (green), 1:10 (yellow) and 1:20 (blue). Experiments were conducted at 25 $^{\circ}$ C, 20 mM Tris-HCl buffer, pH 7.4, 1.25% DMSO. B. TEM images of C2S C7S IAPP control at the end of kinetic study. C. TEM images of C2S C7S IAPP with 20-fold (S)-(+)-Flurbiprofen at the end of kinetic study. Scale bar is 100 nm.

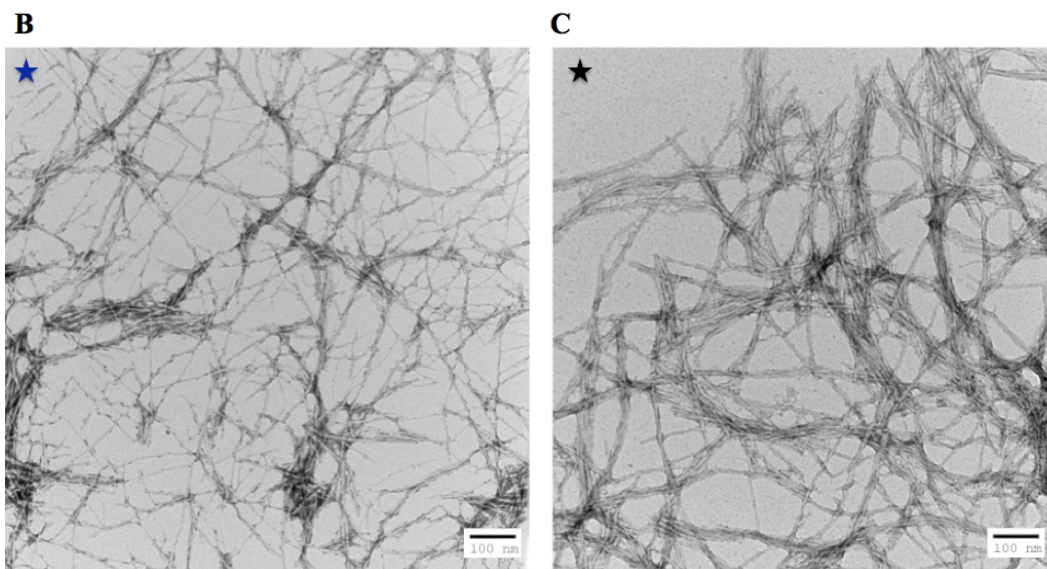
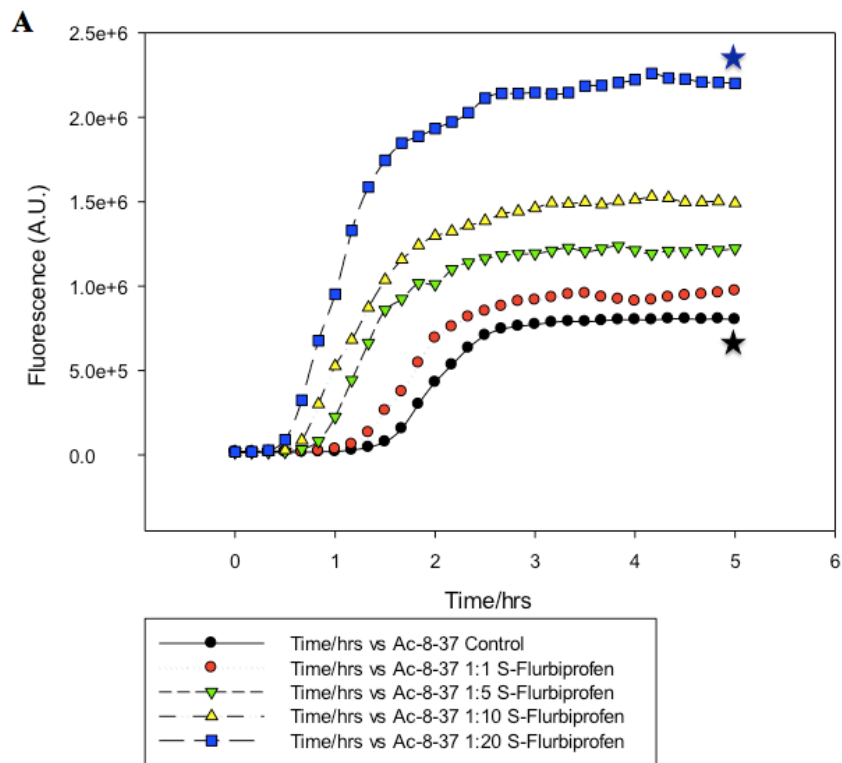


Figure 2-8. Kinetic curves and TEM images of acetylated-8-37 IAPP with and without (S)-(+)-Flurbiprofen. A. Thioflavin-T curves of 16 μM acetylated-8-37 IAPP without (S)-(+)-Flurbiprofen (black), 16 μM 8-37 IAPP at ratio 1:1 (red), 1:5 (green), 1:10 (yellow) and 1:20 (blue). Experiments were conducted at 25 $^{\circ}\text{C}$, 20 mM Tris-HCl buffer, pH 7.4, 1.25% DMSO. B. TEM images of acetylated-8-37 IAPP control at the end of kinetic study. C. TEM images of acetylated-8-37 IAPP with 20-fold (S)-(+)-Flurbiprofen at the end of kinetic study. Scale bar is 100 nm.

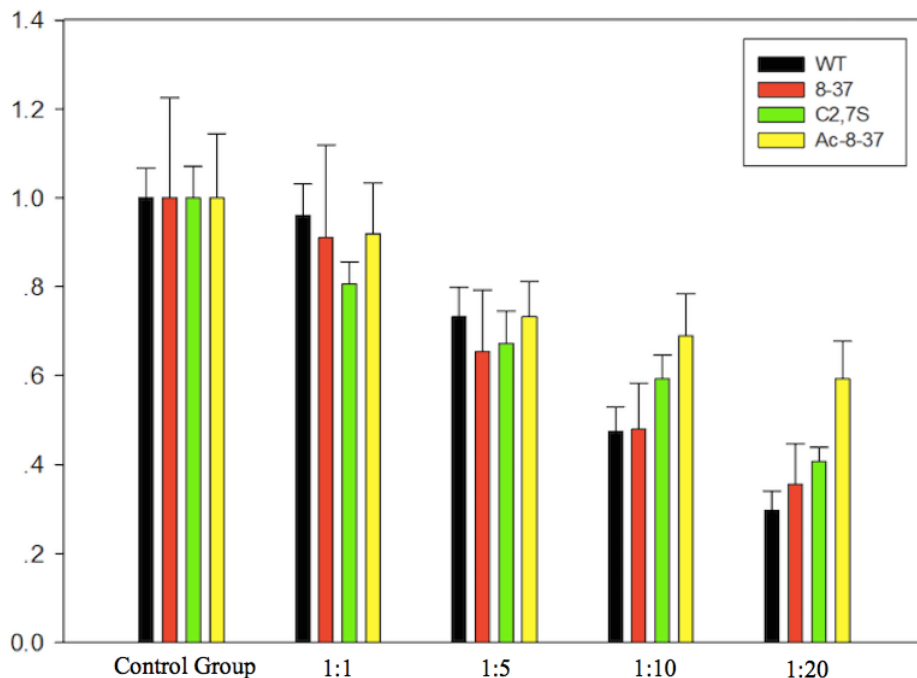


Figure 2-9. Comparison of wild type IAPP (black), 8-37 IAPP (red), C2S C7S IAPP (green), acetylated-8-37 IAPP (yellow) at five concentrations. The value of t_{50} at each ratio is divided by that of control peptide. The t_{50} of control group is set as one. For example, the value of yellow bar at ratio 1:20 is the t_{50} value of acetylated-8-37 IAPP with 20-fold (S)-(+)-Flurbiprofen kinetic curve divided by that of acetylated-8-37 IAPP control. The standard deviation of each condition from 10 duplicates was calculated. The propagation of uncertainty was considered. The error bars representing the combined standard deviation are included in the diagram.

3. Discovery of a New Compound that Accelerates IAPP Amlloid Formation

3.1 Finding New Compounds through DUD-E

Molecular docking screens have been widely used for the discovery of new inhibitors [28-30], but it still remains a challenging task because the total number of structures to be sampled in one screening is so large [31]. One important criterion in the evaluation of docking screens is the enrichment of annotated ligands from among a large database of presumed nonbinding “decoy” structures. The enrichment factor is the concentration of the annotated ligands among the top-scoring docking structures compared to their concentration throughout the entire database [32]. Docking scoring functions can be biased towards physical properties of small molecules such as molecular weight, charge state, cLogP, etc. For example, if the size of ligands are significantly different from that of the decoys, docking enrichments can be artificially good [33]. Thus, the database decoys should resemble the physical properties of the annotated ligands and differ in chemical properties.

Huang and colleagues [32] assembled a directory of useful decoys (DUD) with 2950 ligands for 40 different targets. It is publicly available (<http://dude.docking.org>). They began with 2950 ligands for 40 different proteins taken from the literatures. For each ligand, 36 molecules were chosen from the ZINC database of commercially available “drug-like” compounds [34]. Each of these 36 molecules shared similar physical properties with the particular ligand including molecular weight, cLogP, and the number of hydrogen bonding groups, but differed from the ligand topologically. There were several problems with DUD. For example, net formal charge was imbalanced; 42% of all ligands are charged versus only 15% of the decoys [35]. Later an improved benchmarking set – Directory of Useful Decoys, Enhanced (DUD-E) was proposed [36]. DUD-E addressed several liabilities and developed new

functionality. It has a total of 22,886 active compounds and their affinities against 102 targets. For each active compound, 50 decoys are available with similar physical properties but dissimilar 2-D topology as non-binders. Users can provide their own ligands and generate decoys using the online automated tool (<http://dude.docking.org/generate>). The total amount of the decoys available for the annotated ligand is dependent on the ligand structure. Each time the server provides 50 decoys randomly and the results are sent via e-mail.

Decoys are not supposed to bind to target proteins or other receptors. However, some decoys appear to bind and this may be a source for new inhibitor discovery [37]. Decoys share similar physical properties with known ligands, which explains why some decoys may have potentialities in binding targets. By using the online DUD-E tool, 200 decoys for (S)-(+)-Flurbiprofen were generated. Five of these were purchased because they have reasonable prices and are commercially available from trusted suppliers (Figure 3-1). The wild type kinetics were studied in the presence of 4-[(4-chlorophenyl) thio] thiophene-3-carboxylic acid, 4-(2,4-dimethylphenyl)-2,2,3-trimethylcyclopentanecarboxylic acid, alpha-(3-chloro-6-methylphenylimino)-P-cresol and 2-(2-hydroxyphenyl) benzothiazole respectively. (3-(4-methylphenyl) cyclohexyl) acetic acid, cyclohexylamine salt was not tested because it has a poor solubility in DMSO. 4-[(4-chlorophenyl) thio] thiophene-3-carboxylic acid was found to be able to accelerate IAPP amyloid formation. This compound will be designated as compound A for the rest of this chapter.

3.2 Materials and Methods

3.2.1 Peptide Synthesis

Human IAPP and I26P (shown in Figure 3-2) were synthesized using a CEM microwave assisted peptide synthesizer on 0.1 mmol scale with 9-fluorenylmethoxycarbonyl (Fmoc)

chemistry. Fmoc-protected pseudoproline (oxazolidine) dipeptide derivatives were used as described [26]. Solvents were ACS-grade. Fmoc- Polyethylene glycol- polystyrene (Fmoc-PAL-PEG-PS) resin was used to provide an amidated C-terminus. Standard Fmoc reaction cycles were used. The first residue, Tyr, attached to the resin, pseudoproline dipeptide derivatives, all β -branched residues and all residues directly following a β -branched residue were double coupled. Peptides were cleaved from the resin using standard TFA (trifluoroacetic acid) method. Crude peptides were dissolved in 20% (by volume) acetic acid and lyophilized before oxidation. Then, peptides were oxidized in dimethyl sulfoxide (DMSO) at room temperature[27].

Purification was done via reverse-phase high-performance liquid chromatography (RP-HPLC) with a Higgins C18 preparative column. Analytical HPLC was used to follow the oxidation process. The buffer system consists of buffer A (100% H₂O and 0.045% HCl, by volume) and buffer B (80% acetonitrile, 20% H₂O and 0.045% HCl, by volume). 20%-60% buffer B in 40 minutes was used for the purification of wild type IAPP and I26P-IAPP. The peaks of wild type IAPP and I26P-IAPP appeared from 28 minutes and 26 minutes respectively.

The masses of pure peptides were confirmed by matrix-assisted laser desorption/ionization time-of-flight mass spectrometry (MALDI-TOF MS): wild type IAPP, 3903.3 (expected) and 3903.6 (observed); I26P, 3887.3 (expected) and 3887.2 (observed).

3.2.2 Sample Preparation

Peptide stock solutions were prepared in 100% hexafluoroisopropanol (HFIP) at 1.6mM and filtered through a 0.20 μ m syringe filter. All the stock solutions were stored at -20 °C. The peptide solution was measured into an eppendorf tube and lyophilized for at least 20 hours. The dry peptide was dissolved in 20 mM Tris-HCl buffer to initiate amyloid formation. The final concentration of IAPP in sample solution was 16 μ M.

All the compound tested were purchased from Sigma Aldrich: 4-[(4-chlorophenyl) thio] thiophene-3-carboxylic acid (*CDS017320 ALDRICH*); 4-(2,4-Dimethylphenyl)-2,2,3-Trimethylcyclopentanecarboxylic Acid (*R701025*); (3-(4-Methylphenyl) Cyclohexyl) Acetic Acid, Cyclohexylamine Salt (*L128007*); Alpha-(3-Chloro-6-Methylphenylimino)-P-Cresol (*S684813*); 2-(2-Hydroxyphenyl) benzothiazole (*632589 ALDRICH*). The compounds were dissolved in dimethyl sulfoxide (DMSO) at 128 mM and diluted to 64mM, 32mM and 6.4mM. (3-(4-Methylphenyl) Cyclohexyl) Acetic Acid, Cyclohexylamine Salt cannot be dissolved in DMSO. It did not go through the following tests. The final concentrations of tested compounds were 320 μ M, 160 μ M, 80 μ M, and 16 μ M respectively.

3.2.3 Thioflavin-T Assays

The thioflavin-T assays were performed on a Beckman model D880 plate reader. The excitation filter was 430 nm and emission filter was 485 nm. The experiments were performed in Corning 96-well plate at 25 °C, which was sealed with Corning sealing tape to minimize evaporation.

All the peptides were prepared in hexafluoroisopropanol (HFIP) to a final concentration of 1.6 mM. The HFIP stock solution was filtered through a 0.20 μ m syringe filter to remove seeds. Aliquots of filtered stock solution were distributed into eppendorf tubes and lyophilized. After adding Tris-HCl (20 mM, pH 7.4) buffer, 120 μ l of 32 mM thioflavin-T solution was added before measurements. For experiments without compound, same amount of DMSO was added to the mixture as control. The final concentration of peptide was 16 μ M. The final concentrations of each compound were 320 μ M, 160 μ M, 80 μ M, 16 μ M and 0 μ M respectively. Each sample contained 0.25% DMSO (by volume). The data was analyzed using SigmaPlot v12.

3.2.4 UV Spectrum

The UV absorbance of each compound was tested before conducting kinetic studies to ensure that background absorbance was not an issue. The experiments were performed on a Beckman model DU 730 life science UV/VIS spectrophotometer. The UV absorbance cannot interfere with thioflavin-T assay. Each compound was dissolved in DMSO at 128 mM. Then it was diluted using 20 mM Tris-HCl buffer (pH 7.4) to the final concentration of 320 μ M (similar condition to that used in the thioflavin-T assay, but without peptide added). The sample contains 0.25% DMSO. λ_{max} of DMSO is 275 nm. If the absorbance of the compound does not interfere with thioflavin-T assay (excitation 430nm, emission 485nm), it can be tested using thioflavin-T assay.

3.2.5 Transmission Electron Microscopy (TEM)

TEM images were collected at the Life Science Microscopy Center at Stony Brook University. 15 μ l of the sample from the end of each kinetics study was placed on a carbon-coated 300 mesh copper grid for 1 minute, and then negatively stained with saturated uranyl acetate for 1 minute.

3.2.6 ^1H NMR

The samples of compounds were collected in 20 mM Deuterium-Tris DCl buffer (pD 7.8). The final concentrations were 16 μ M and 320 μ M respectively. ^1H NMR data was collected using 500 MHz Bruker NMR spectrometer. The relaxation time was set to 40 seconds. The DOSY experiment was used to determine the diffusion coefficient. 1,4-dioxane was used as an internal standard. The final solution contained 0.025% 1,4-dioxane.

3.2.7 Preparation of Vesicles

Vesicles were composed of 100% DOPG. Stock solutions of DOPG were mixed and dried under vacuum overnight. The resulting lipid film was hydrated in 20 mM Tris-HCl buffer (pH 7.4) for 1 hour. The lipid concentration was 2.5 mM. Multilamellar vesicles were then subjected to 6 freeze-thaw cycles and extruded 15 times through 100 nm pore size filters (Whatman, GE). The final concentration was 48 μ M.

3.3 Results and Discussion

3.3.1 4-[(4-chlorophenyl) thio] thiophene-3-carboxylic acid (Compound A) Accelerates Amyloid Formation by Wild Type IAPP, But the Other Compounds Have No Effect

Five compounds were purchased and four of them could be tested. The fifth compound, (3-(4-Methylphenyl) Cyclohexyl) Acetic Acid, Cyclohexylamine Salt had poor solubility in DMSO. So it could not be tested in this thesis. Preliminary data was recorded at a ratio of 1:20 of wild type IAPP and each compound. The solutions contained 20 mM Tris-HCl buffer at pH 7.4, 16 μ M wild type IAPP, 32 μ M thioflavin-T and 0.25% DMSO. In the control group only DMSO was added. In the tested group the compound was dissolved in DMSO and added to the solution to a final concentration of 320 μ M. 4-[(4-chlorophenyl) thio] thiophene-3-carboxylic acid (compound A) was able to accelerate wild type IAPP amyloid formation (shown in Figure 3-3). It has effects that are similar with (S)-(+)-Flurbiprofen. The findings with compound A may provide more information in understanding the binding mechanism of (S)-(+)-Flurbiprofen. The kinetic studies of the other three compounds are shown in APPENDIX.

It is important to make sure that the absorbance of the compound does not interfere with thioflavin-T assay. Several compounds have been reported to be able to affect thioflavin-T fluorescence [38]. A UV scan of 320 μ M compound A was performed. The sample contained

0.25% DMSO so the UV absorption of DMSO should be considered. The results are shown in Figure 3-4. There are two major peaks: λ_{\max} 280 nm and λ_{\max} 300 nm. The UV absorbance under the experimental condition does not interfere with the thioflavin-T assay.

Thioflavin-T assays of IAPP with compound A at different concentrations were conducted. The results are shown in Figure 3-5 A. The concentration dependent experiment (Figure 3-4 B) exhibits a similar pattern to that previously seen with (S)-(+)-Flurbiprofen. Compound A had little impact on the fibril formation at a 1:1 ratio. At higher concentrations, the effect of compound A on wild type IAPP fibril formation was more apparent. The lag phase of the fibril formation process is shorter when more compound A was added. The final intensity with compound A also increased compared to that of the wild type IAPP itself. Fibrils formed in the presence of 20-fold compound A was collected. TEM images of these fibrils were taken (Figure 3-5 B, C). There was no significant change in morphology.

In order to compare the effect of compound A, the value of t50 at each concentration was calculated. The t50 value is defined here as the time point when the kinetic curve reaches half of its final intensity during a thioflavin-T assay. The t50 value of each concentration was divided by that of the wild type IAPP control group and the data was plotted as normalized t50. The bar graph is shown in Figure 3-6. For ratios 1:1 to 1:20 of peptide to compound A, the t50 values were $90\pm 4\%$, $61\pm 13\%$, $33\pm 8\%$ and $17\pm 3\%$ of that of the control group respectively.

3.3.2 Compound A Does Not Aggregate

NMR experiments can be used to detect compound aggregation. Resonance number, peak shape and shifts may change if aggregate species exist. Peak intensities mainly correlate with concentrations [39]. In order to test whether compound A aggregates, samples were prepared in 20 mM Deuterium-Tris DCl buffer at 16 μ M and 320 μ M and the spectrum were compared.

Compound A could not be dissolved in D₂O or acidic solution. 1,4-dioxane (0.025% by volume) was added as internal standard. The results are shown in Figure 3-7. As the concentration changed from 16 μM to 320 μM, the number of resonance, chemical shifts and the shape of the peaks did not change. Only the intensities changed. The large peak appearing at 3.7 ppm belongs to 1,4 dioxane. The calculated concentration of 320 μM sample is 340 μM by using the concentration of 1,4-dioxane as an internal standard. Considered the accuracy of instruments, the error is within a reasonable range. This indicates that the compound is soluble in the experimental condition.

The DOSY experiment was used to determine the diffusion coefficient. The basic equation used in the experiment is $R_{h,1}/R_{h,2} = D_{\text{coefficient},2}/D_{\text{coefficient},1}$. 1,4-dioxane was used as an internal standard for the known $R_{h,2} = 2.12 \text{ \AA}$. From the DOSY experiment, $D_{\text{coefficient},2}$, $D_{\text{coefficient},1}$ were obtained. $R_{h,1} = R_{h,2} * D_{\text{coefficient},2}/D_{\text{coefficient},1}$ and $R_{h,\text{compound A}} = 3.6 \text{ \AA}$. The R_g is 2.9 Å predicted by HYDROPRO. Calculated from $R_g = 0.75R_h$, the predicted $R_{h,\text{compound A}}$ is 3.9 Å, which is in accordance with the experimental result. If compound A aggregates in solution, the experimental $R_{h,\text{compound A}}$ could be much larger than the predicted value.

The point-mutant I26P-IAPP itself does not form amyloid. However, it can do so if lipid vesicles are present. If compound A aggregates and forms micelle-like structure, it may catalyze amyloid formation by I26P as lipid vesicles. Thus compound A was tested with I26P-IAPP (Figure 3-8). Thioflavin-T kinetic studies suggest that no amyloid is formed by I26P-IAPP in the presence of compound A. The result indicates that compound A does not form aggregates in experimental condition.

3.4 Conclusions

Compound A has been found to be able to accelerate fibril formation without changing the

fibril morphology. Compound A was discovered through generating decoys of (S)-(+)-Flurbiprofen. These decoys had similar molecular weight, charge, calculated cLogP, etc, but they are topologically different from known ligands. Thus the findings of compound A offer a new starting point for developing compounds that modulate the rate of IAPP amyloid formation.

Compound A and (S)-(+)-Flurbiprofen can accelerate IAPP amyloid formation and increase final intensity in thioflavin-T assays. Although compound A and (S)-(+)-Flurbiprofen share similar physical features and functionality, it is possible that they have different mechanisms in binding. Their effects on thioflavin-T assay are also worthy of exploration. It will be interesting to see how compound A affects cell viability and to see if it inhibits toxicity.

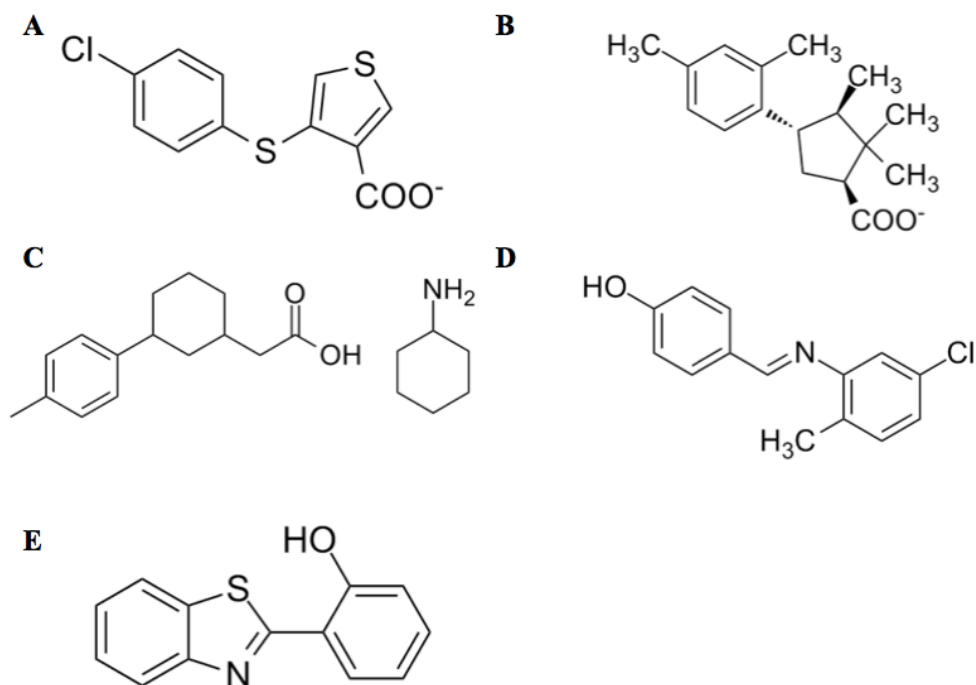


Figure 3-1. Decoys generated from DUD-E (<http://decoys.docking.org>) and purchased from Sigma-Aldrich. A. 4-[4-chlorophenyl] thio] thiophene-3-carboxylic acid B. 4-(2,4-Dimethylphenyl)-2,2,3-Trimethylcyclopentanecarboxylic Acid C. (3-(4-Methylphenyl) Cyclohexyl) Acetic Acid, Cyclohexylamine Salt D. Alpha-(3-Chloro-6-Methylphenylimino)-P-Cresol E. 2-(2-Hydroxyphenyl) benzothiazole

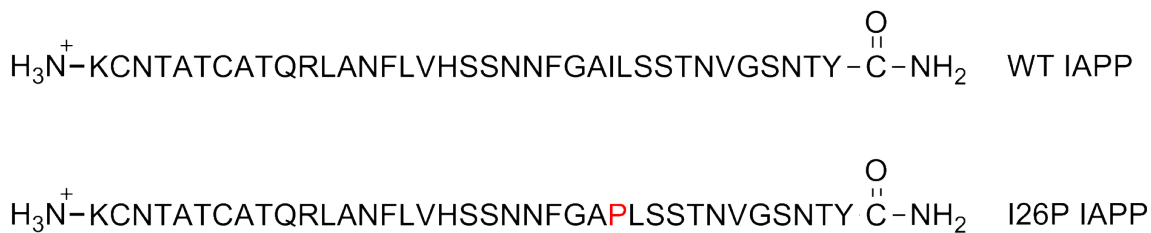


Figure 3-2. Primary sequences of wild type human IAPP and the IAPP mutant I26P.

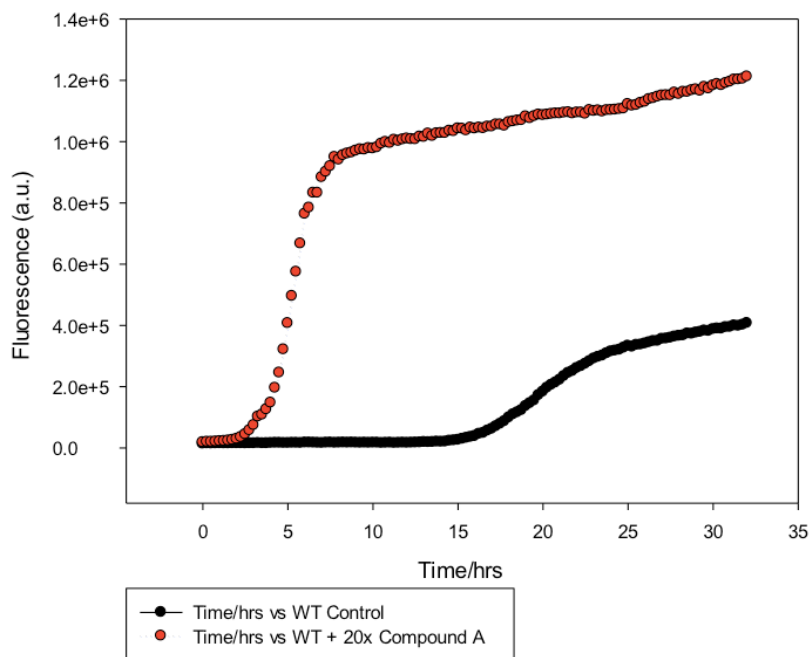


Figure 3-3. Thioflavin-T curves of wild type IAPP compared to that of same peptide with 20-fold excess of 4-[(4-chlorophenyl) thio] thiophene-3-carboxylic acid. Experiments were conducted at 25 °C, 20 mM Tris-HCl buffer, pH 7.4, 0.25% DMSO. 20-fold excess of compound A can shorten the lag phase of amyloid formation while increasing the final intensity.

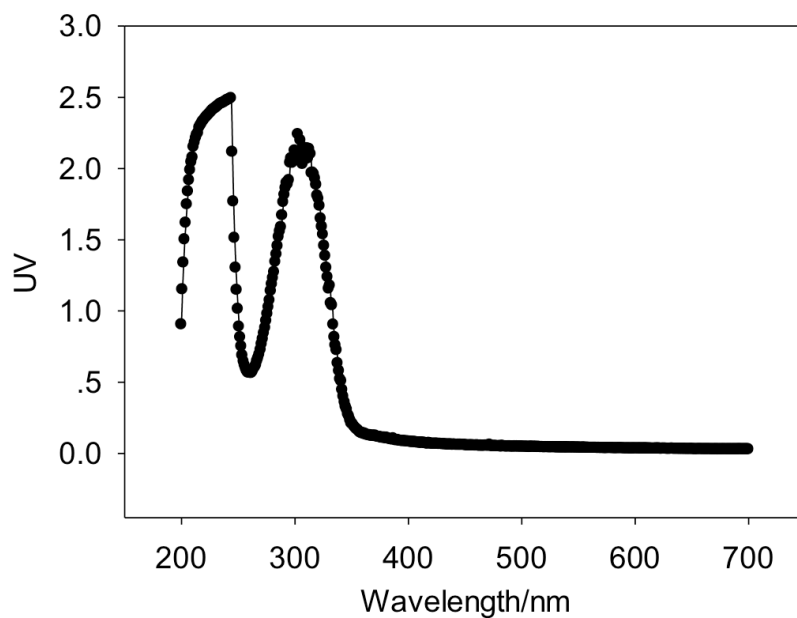


Figure 3-4. UV scan of compound A from 700 nm to 200 nm. The concentration of compound A was 320 μ M. The sample contained 0.25% DMSO. The UV absorption of compound A does not interfere with thioflavin-T.

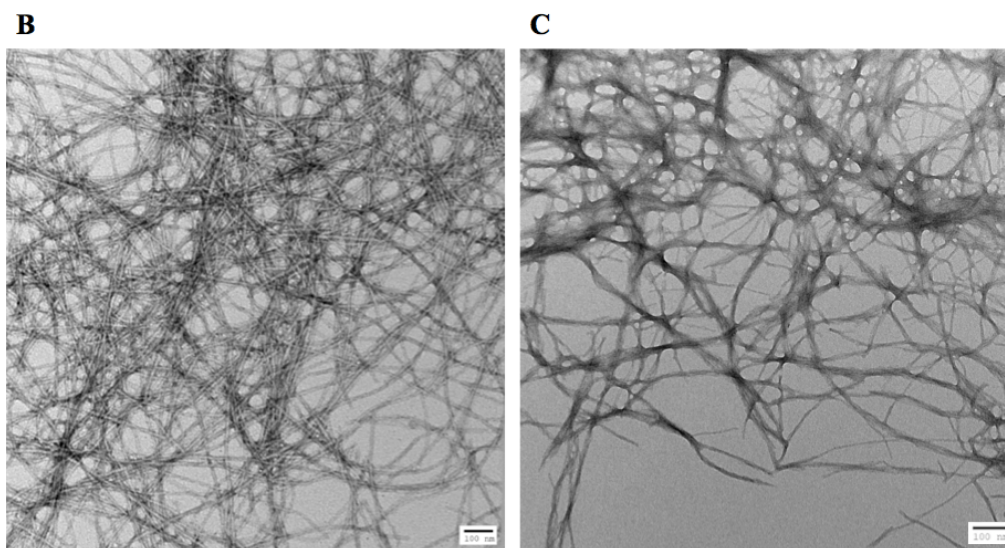
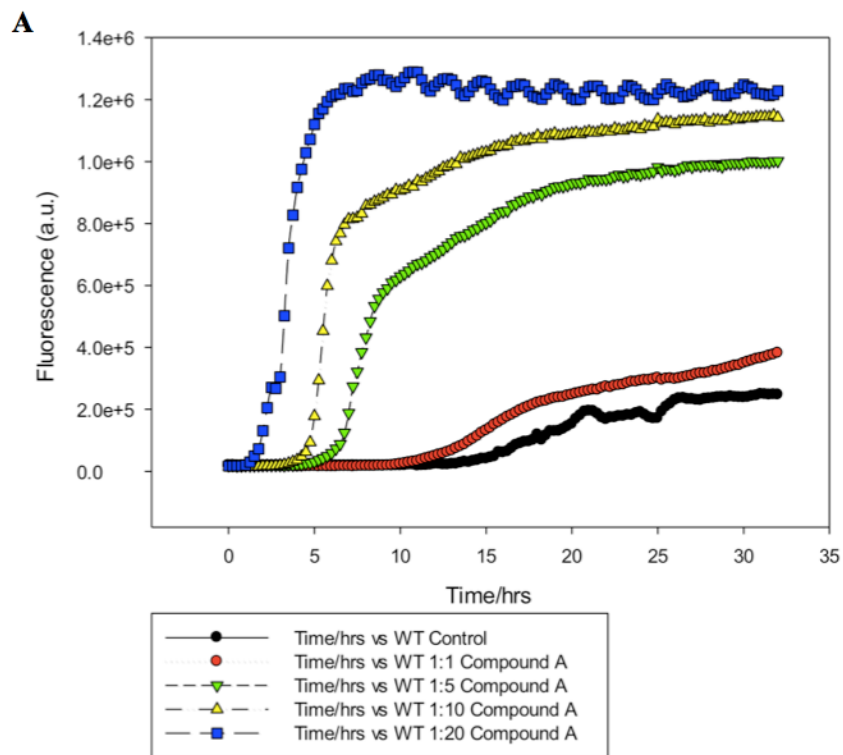


Figure 3-5. Kinetic curves and TEM images of wild type IAPP and 4-[(4-chlorophenyl) thio] thiophene-3-carboxylic acid. A. Thioflavin-T curves of 16 μ M wild type IAPP without compound A (black), with compound A at ratio 1:1 (red), 1:5 (green), 1:10 (yellow) and 1:20 (blue). Experiments were conducted at 25 $^{\circ}$ C, 20 mM Tris-HCl buffer, pH 7.4, 0.25% DMSO. B. TEM images of wild type IAPP control at the end of kinetic study. C. TEM images of wild type IAPP with 20-fold compound A at the end of kinetic study. Scale bar is 100 nm.

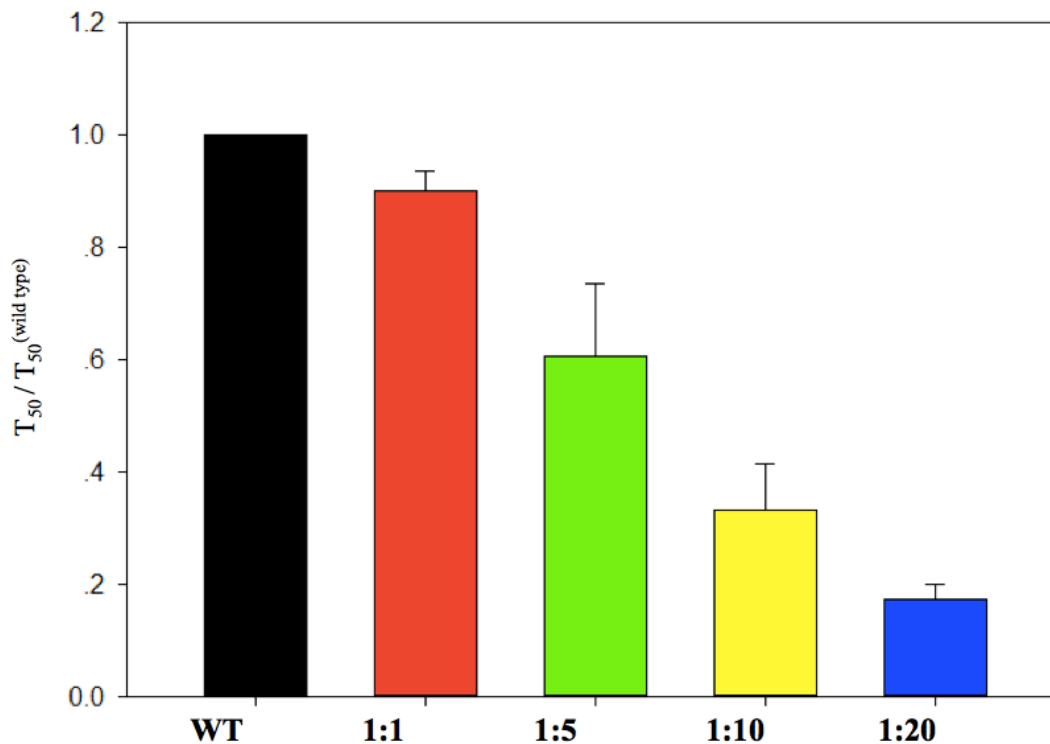
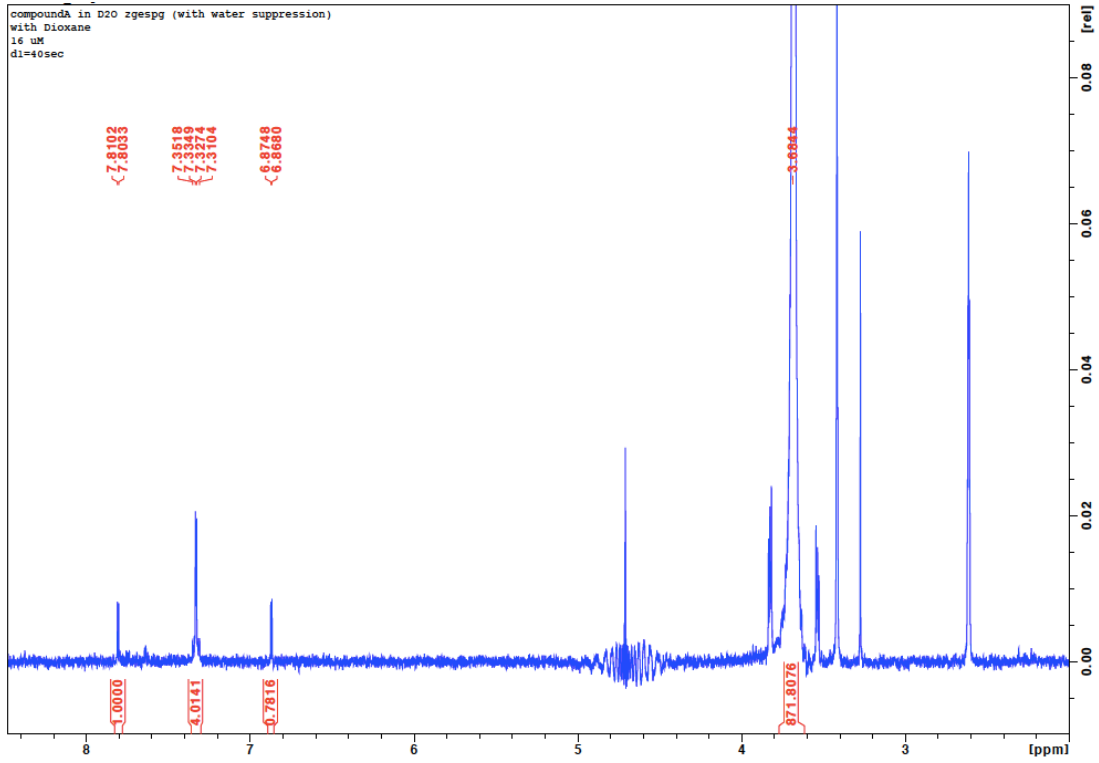
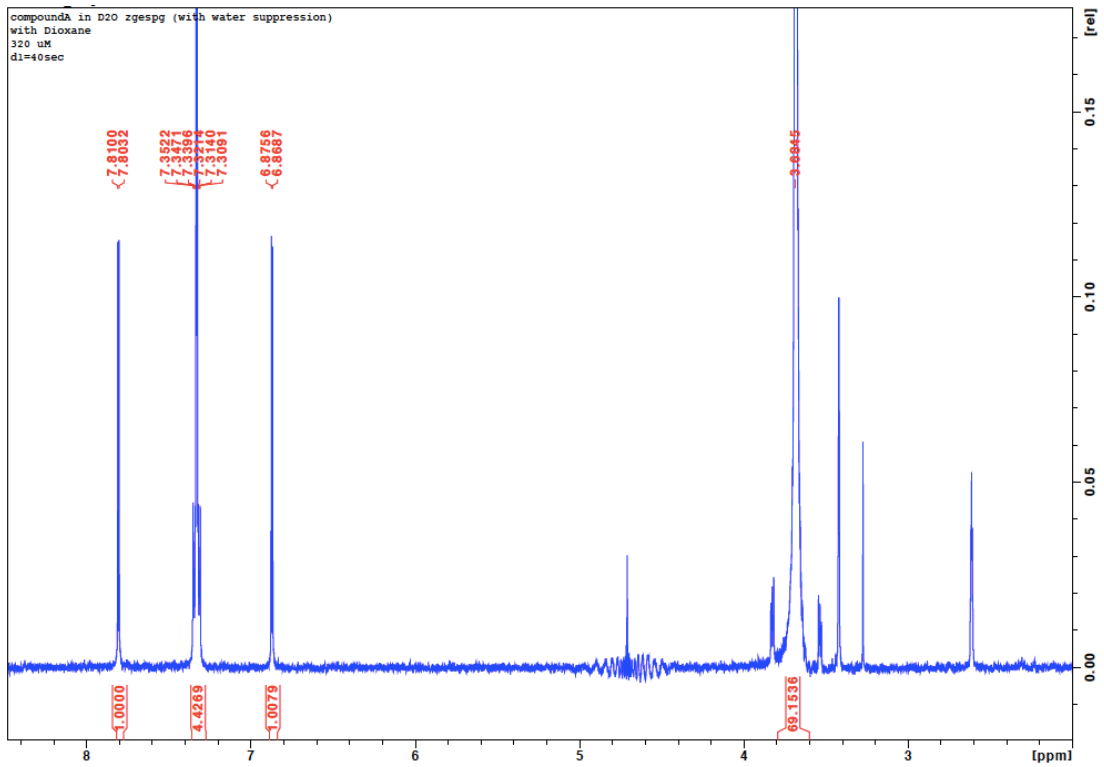


Figure 3-6. T50 value comparison. The t50 value of each concentration was divided by that of the wild type IAPP control group. Compound A is able to accelerate amyloid formation by wild type IAPP. The standard deviation of each condition from 6 duplicates was calculated. The propagation of uncertainty was considered. The error bars representing the combined standard deviation are included in the diagram.

A



B



C

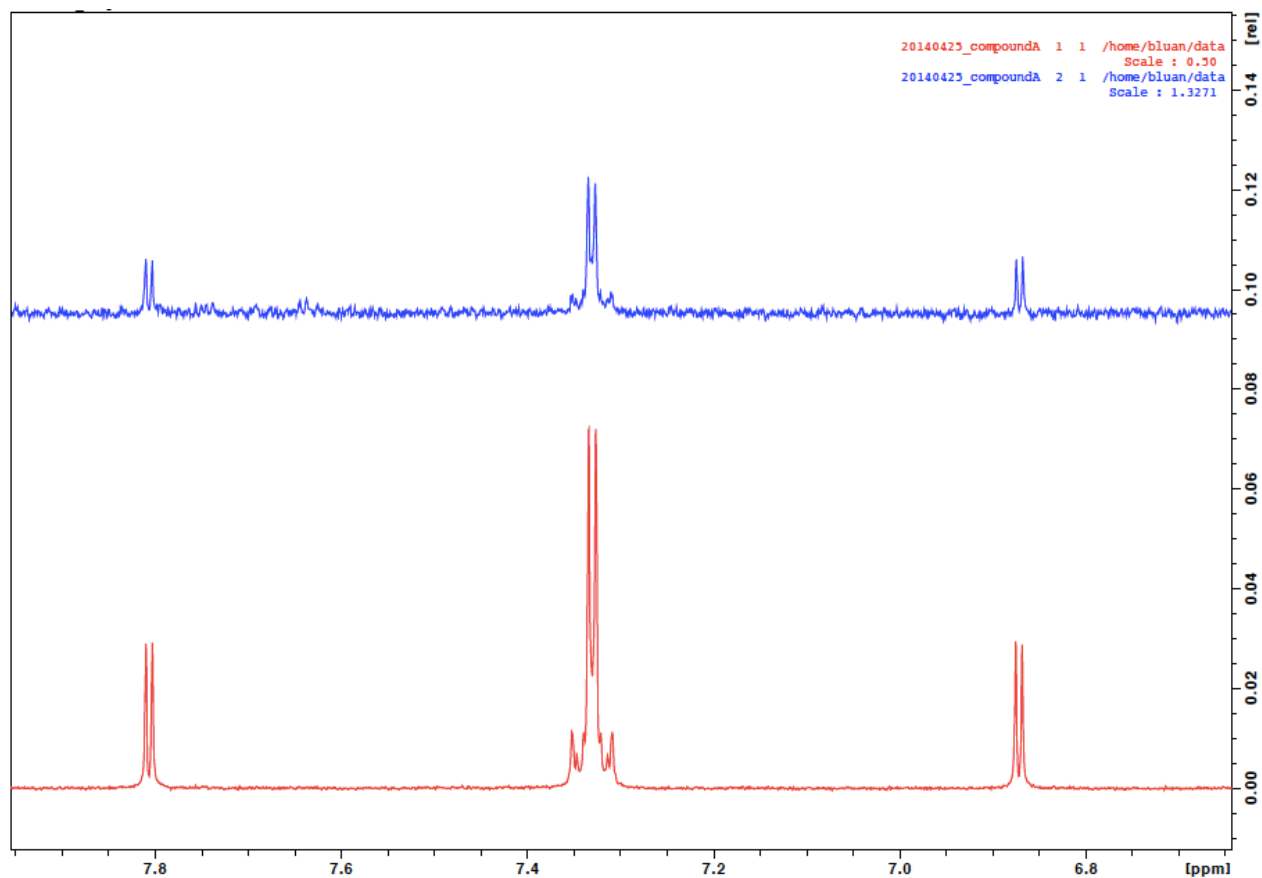


Figure 3-7. NMR spectrum of 4-[(4-chlorophenyl)thio]thiophene-3-carboxylic acid. A. NMR spectrum of compound A at 16 μM B. NMR spectrum of compound A at 320 μM . C. Overlap of A and B. The resonance numbers, shifts and shape are in accordance with the structure of compound A. The intensities increase at higher concentration.

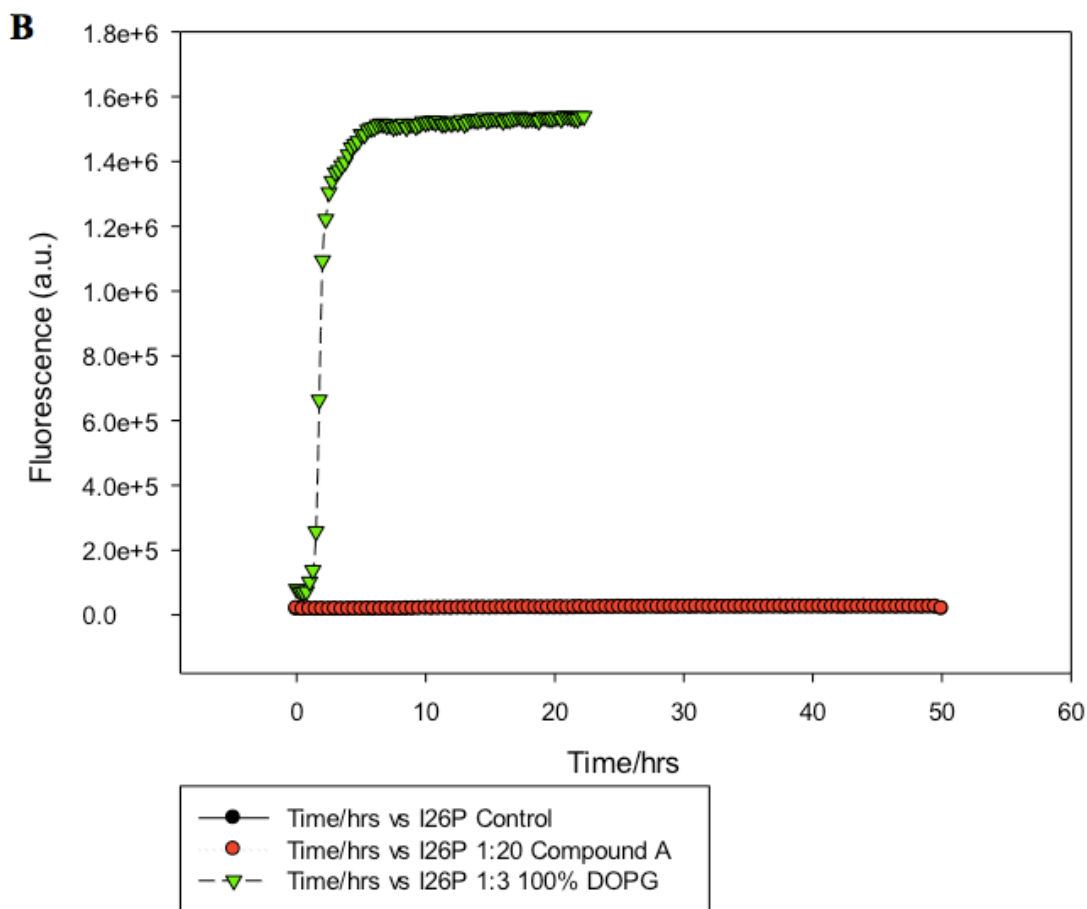
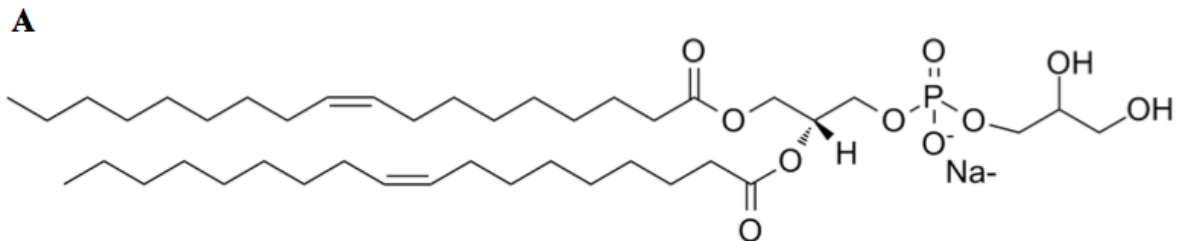


Figure 3-8. Structure of DOPG and kinetic curves of I26P-IAPP in the presence and absence of DOPG. A. DOPG structure. B. The kinetic curves of I26P-IAPP itself as the control group, I26P-IAPP with 20-fold compound A and I26P-IAPP with 3-fold 100% DOPG vesicles. The concentration of wild type IAPP was 16 μ M. 20-fold compound A cannot induce fibril formation of I26P (curves overlap). The sample was kept for 7 days and no change in the fluorescence signal was observed (data after 50 hours is not shown). 100% DOPG can form anionic vesicles and induce I26P fibril formation.

Appendix

4-(2,4-Dimethylphenyl)-2,2,3-Trimethylcyclopentanecarboxylic Acid, alpha-(3-Chloro-6-Methylphenylimino)-P-Cresol and 2-(2-Hydroxyphenyl) benzothiazole were tested in this thesis. UV scan of each compound from 700 nm to 200 nm was conducted. Thioflavin-T studies were conducted at 25 °C, 20 mM Tris-HCl buffer, pH 7.4, 0.25% DMSO. The results are shown in Figure 4-1, 4-2 and 4-3.

Table 1 includes the structures of the 200 decoys.

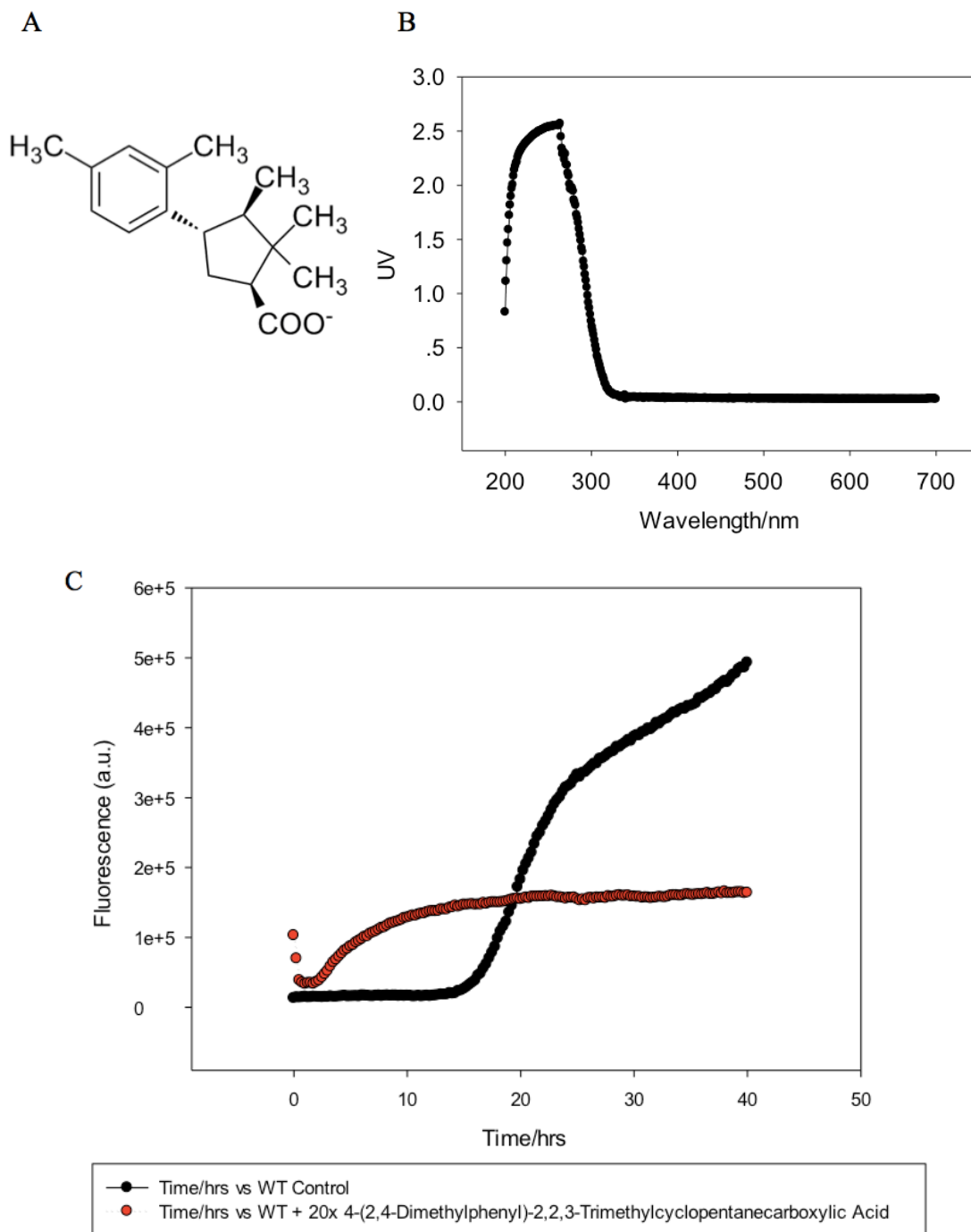


Figure 4-1. Kinetic curves of wild type IAPP with and without 4-(2,4-Dimethylphenyl)-2,2,3-Trimethylcyclopentanecarboxylic Acid. A. Compound structure of 4-(2,4-Dimethylphenyl)-2,2,3-Trimethylcyclopentanecarboxylic Acid B. UV scan from 700 nm to 200 nm C. Thioflavin-T curves of 16 μ M wild type IAPP without the compound (black), with the compound at ratio 1:20 (red). Experiments were conducted at 25 $^{\circ}$ C, 20 mM Tris-HCl buffer, pH 7.4, 0.25% DMSO. *NOTE*: It is not clear if the curve of the sample with 20-fold excess of the compound would eventually reach the final intensity of the wild type IAPP. The wild type IAPP sample had normal-length lag phase. But the final intensity did not reach a plateau.

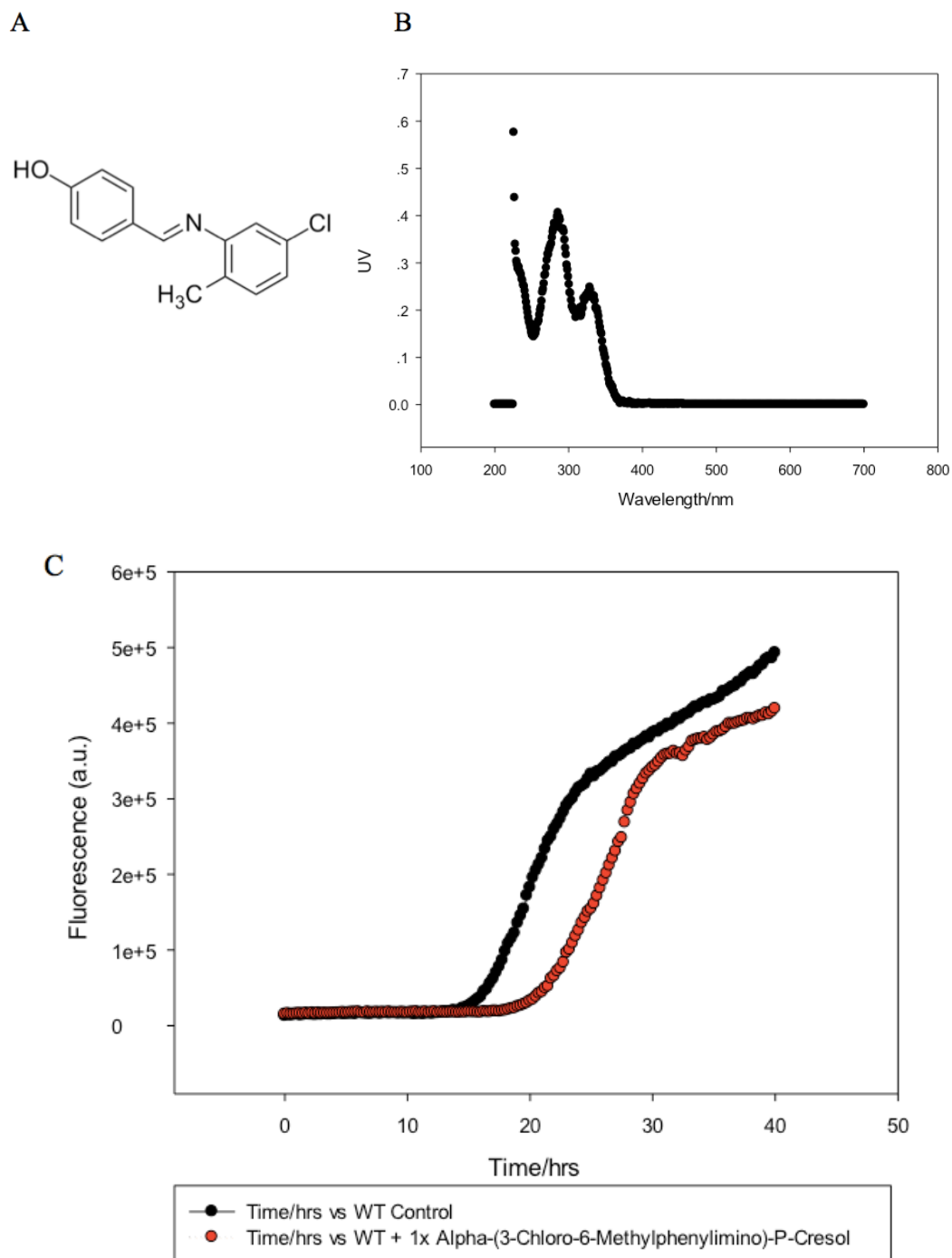


Figure 4-2. Kinetic curves of wild type IAPP with and without alpha-(3-Chloro-6-Methylphenylimino)-P-Cresol. Compound structure of alpha-(3-Chloro-6-Methylphenylimino)-P-Cresol B. Thioflavin-T curves of 16 μ M wild type IAPP without the compound (black), with the compound at ratio 1:1 (red). Experiments were conducted at 25 $^{\circ}$ C, 20 mM Tris-HCl buffer, pH 7.4, 0.25% DMSO. *NOTE*: The wild type IAPP sample had normal-length lag phase. But the final intensity did not reach a plateau. The compound was only tested at the ratio 1:1.

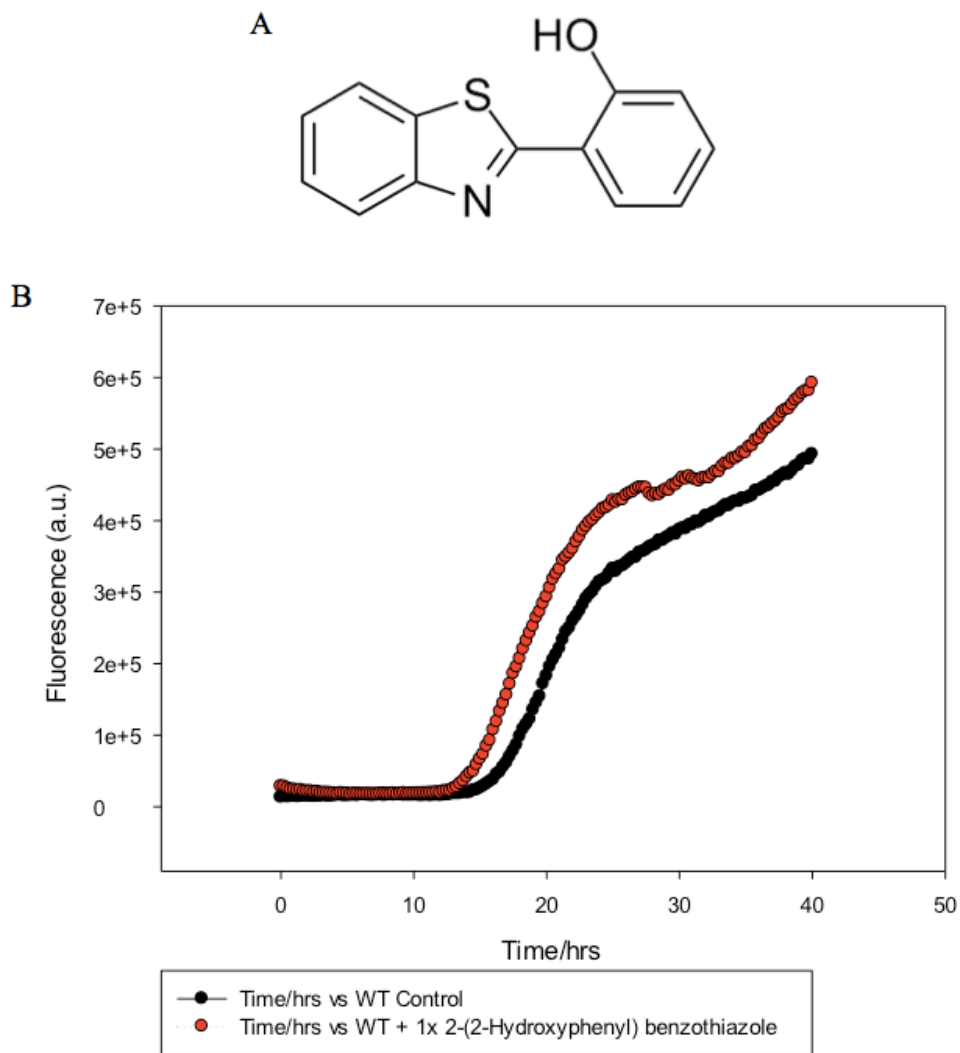
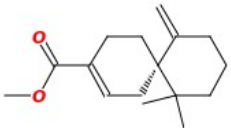
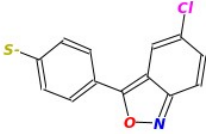
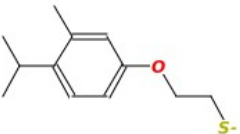
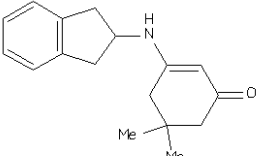
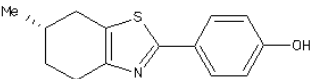
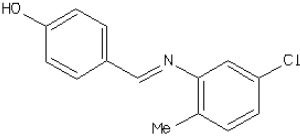
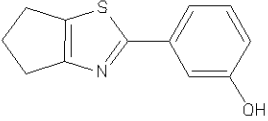
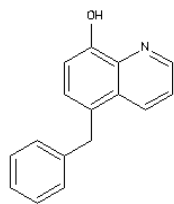


Figure 4-3. Kinetic curves of wild type IAPP with and without 2-(2-Hydroxyphenyl) benzothiazole. A. Compound structure of 2-(2-Hydroxyphenyl) benzothiazole B. Thioflavin-T curves of 16 μ M wild type IAPP without the compound (black), with the compound at ratio 1:1 (red). Experiments were conducted at 25 $^{\circ}$ C, 20 mM Tris-HCl buffer, pH 7.4, 0.25% DMSO. *NOTE*: The wild type IAPP sample had normal-length lag phase. But the final intensity did not reach a plateau. The compound was only tested at the ratio 1:1.

Table 1. List of 200 Decoys

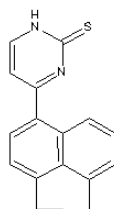
Number	Decoy Structure	ZINC Code	
1		13385395	
2		16789759	
3		19803968	
4		09356348	
5		20432953	
6	<p>(Available from Sigma Aldrich: 100 USD/250mg)</p>		02143588
7		26514528	

8



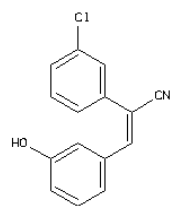
01664763

9



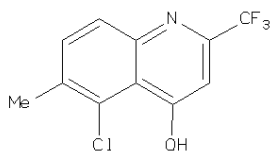
31808357

10



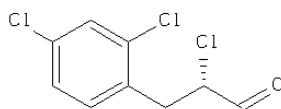
31934947

11



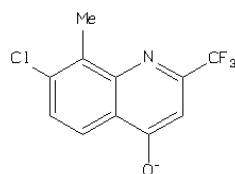
16159566

12



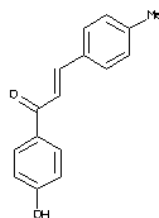
36205323

13



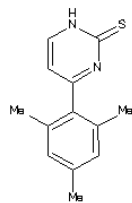
36912540

14



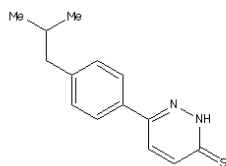
05102183

15



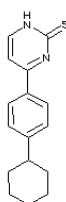
41256493

16



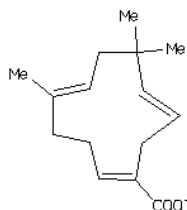
41291215

17



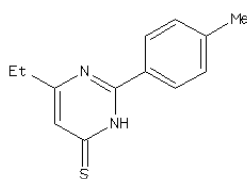
41392424

18



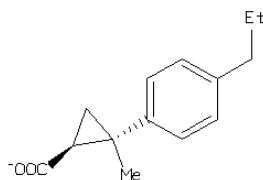
44143865

19



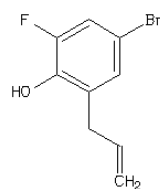
45956088

20



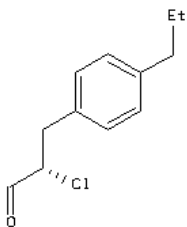
49816698

21



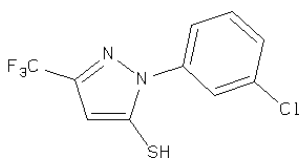
52064439

22



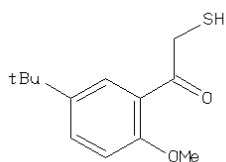
52228245

23



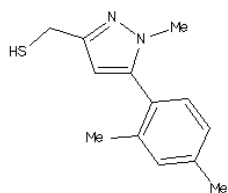
52305108

24



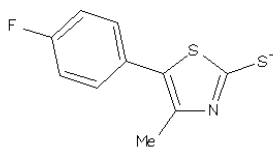
57529462

25



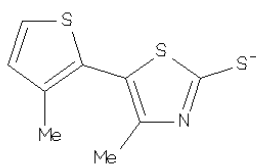
57953706

26



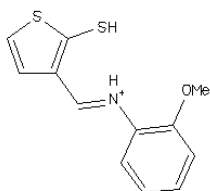
58003711

27



58003864

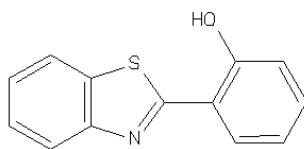
28



00251276

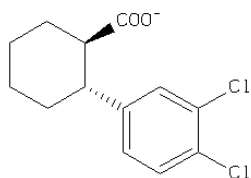
29

(Available from Sigma
Aldrich: 29.2 USD/5g)



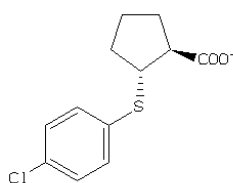
00235985

30



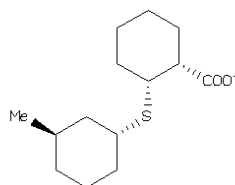
62666660

31



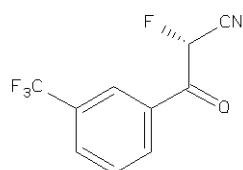
62764506

32



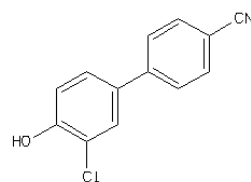
62767402

33



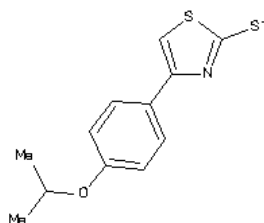
63110812

34

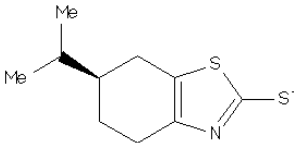
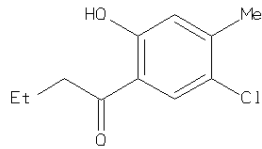
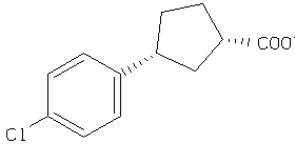
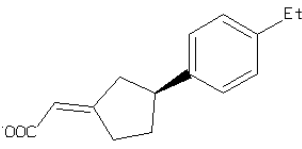
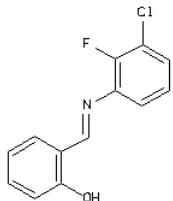
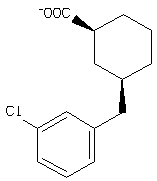
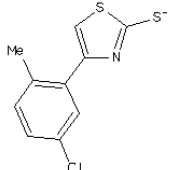


65343074

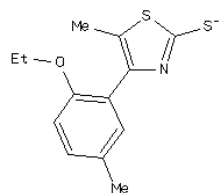
35



70598274

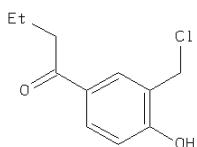
36		70598298
37 (no vendor)		71454581
38 (no vendor)		71531868
39 (no vendor)		71534716
40		05290523
41		75202323
42		75420674

43



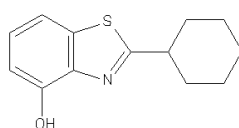
75420713

44



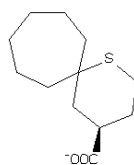
75622222

45



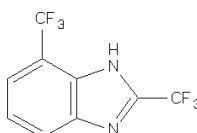
75841355

46



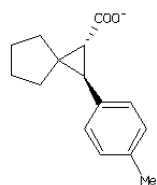
76063724

47



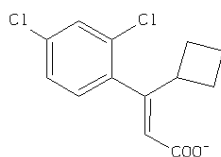
76214040

48



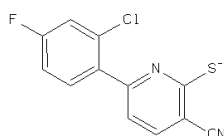
76677306

49



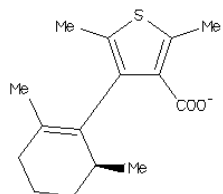
76710806

50



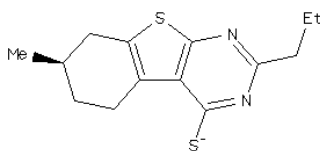
78940171

51



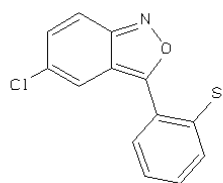
04019227

52



04910705

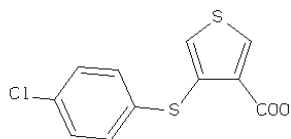
53



05032109

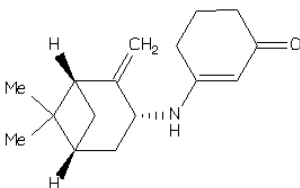
54

(Available from Sigma
Aldrich: 50 USD/25 mg)



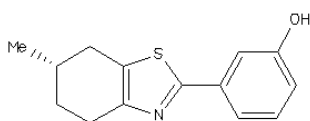
00149027

55



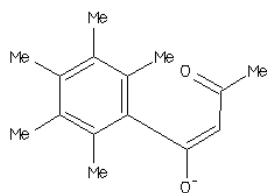
03984455

56



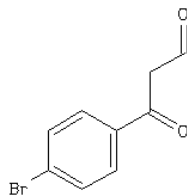
20432981

57



03847968

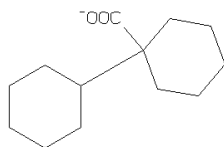
58



01669695

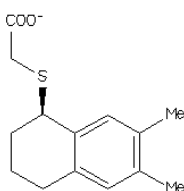
59

(Available from Sigma
Aldrich: 100 USD/1mg)



31361588

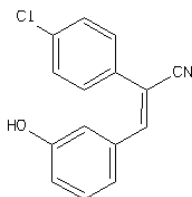
60



31889376

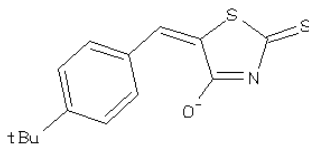
61

(no vendor)



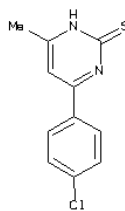
31934951

62



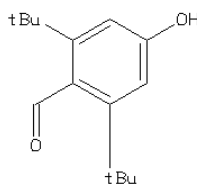
02536883

63



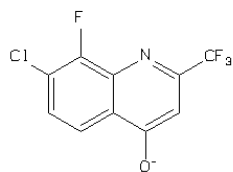
00157497

64



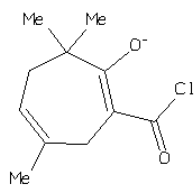
34751495

65



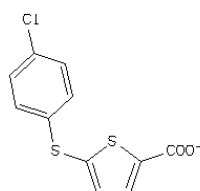
36912416

66



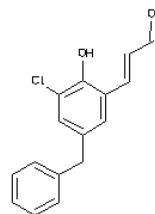
39055840

67



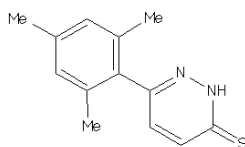
40541648

68



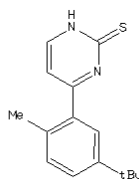
40546380

69



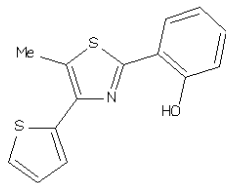
41256499

70



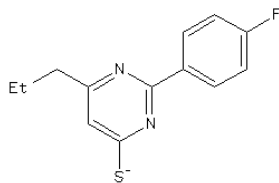
41343101

71



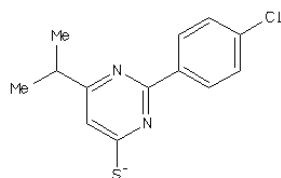
42410690

72



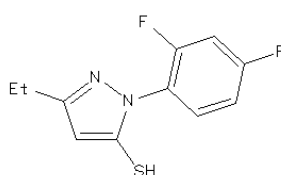
45956304

73



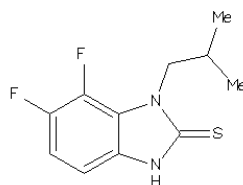
45956320

74



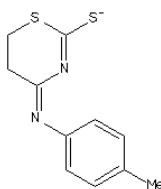
52304893

75



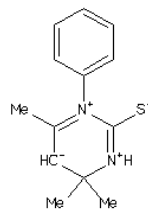
53168696

76



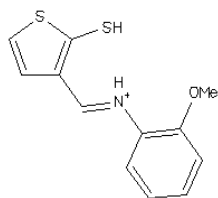
39886274

77

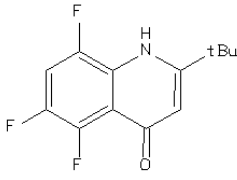
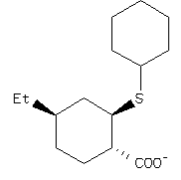
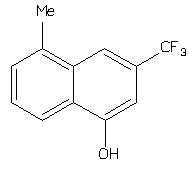
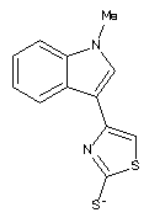
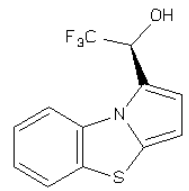
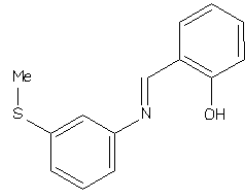
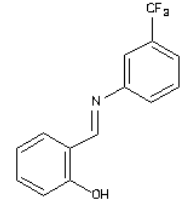


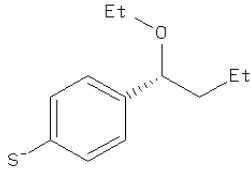
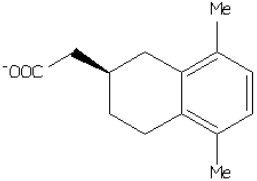
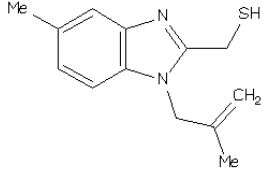
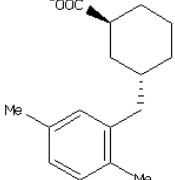
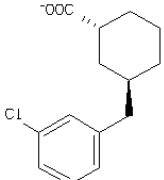
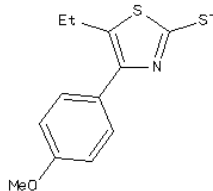
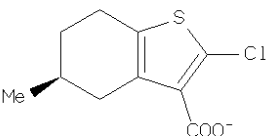
56634894

78

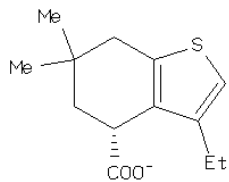


00251276

79		61094904
80		62766323
81		64220153
82 (no vendor)		71560972
83 (Available from Sigma Aldrich: 250 USD/25mg)		71781982
84 (Available from Sigma Aldrich: 100 USD/250mg)		02163597
85		17429034

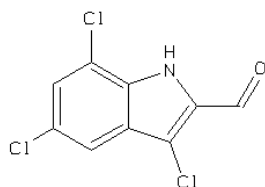
86		72220250
87 (no vendor)		74082882
88 (no vendor)		74295648
89 (no vendor)		75186301
90 (no vendor)		75202325
91 (no vendor)		75420767
92 (no vendor)		75464457

93
(no vendor)



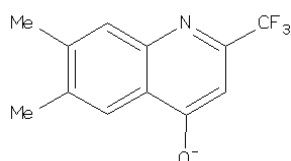
75628814

94
(no vendor)



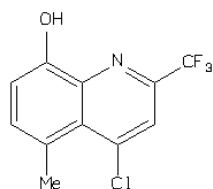
75775815

95
(no vendor)



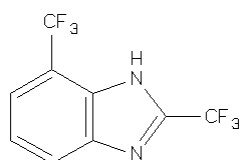
75893458

96
(no vendor)



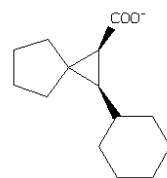
75893727

97



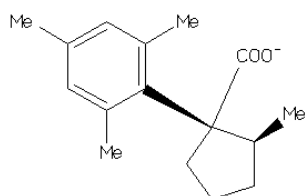
76214040

98
(no vendor)

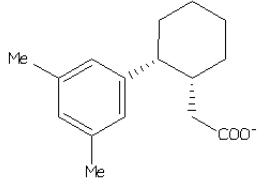
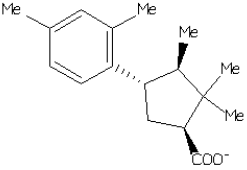
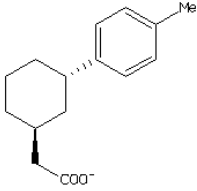
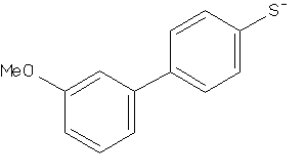
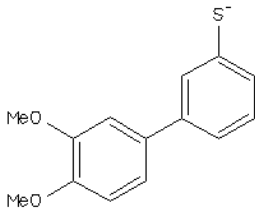
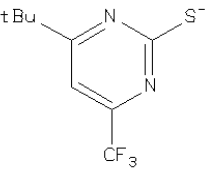
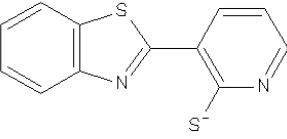


76672500

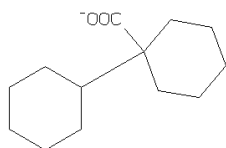
99
(no vendor)



77402526

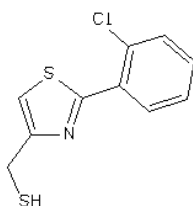
100 (no vendor)		77402596
101 (Available from Sigma Aldrich: 100 USD/25mg)		00122195
102 (Available from Sigma Aldrich: 80 USD/1EA)		00392281
103		15441828
104		15441838
105		06882834
106		22161930

107



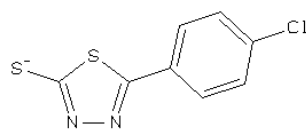
31361588

108



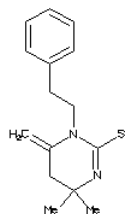
31890204

109



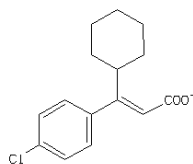
02574872

110



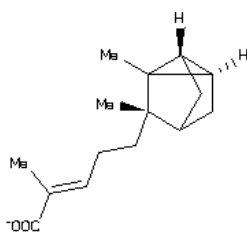
36046704

111



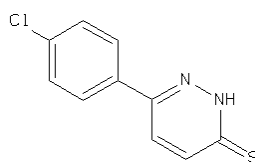
36174061

112



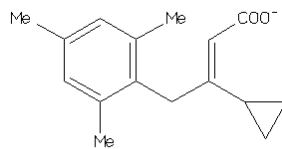
13660029

113



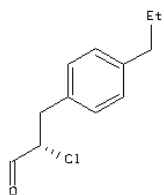
39236981

114



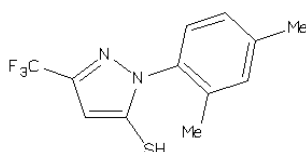
41290645

115



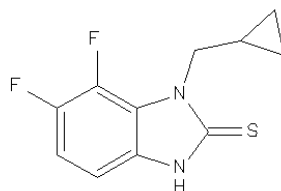
52228245

116



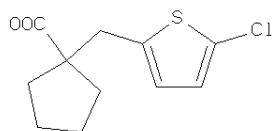
52305301

117



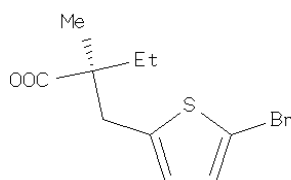
53168590

118



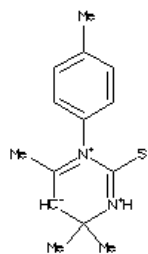
54632515

119



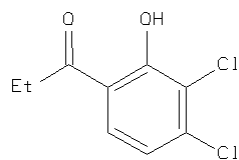
54633586

120



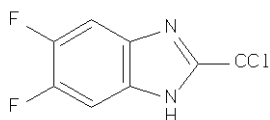
56635564

121



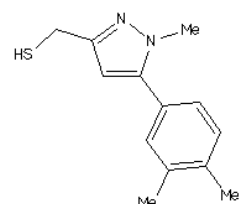
57218731

122



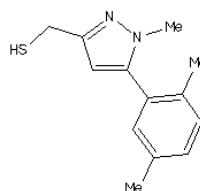
57798061

123



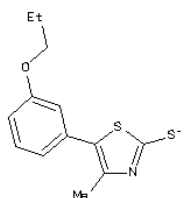
57953701

124



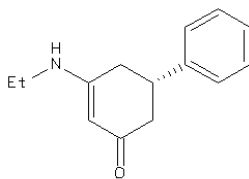
57953703

125



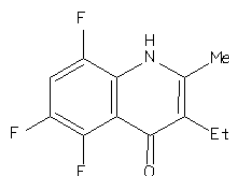
58002560

126



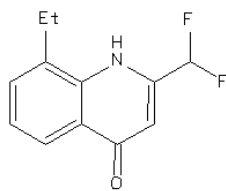
58836381

127



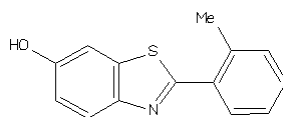
61094908

128



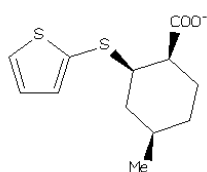
61629415

129



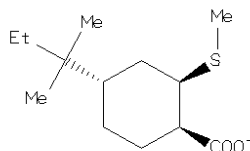
62200062

130



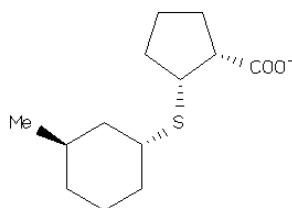
62764327

131



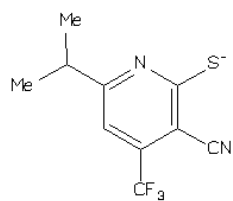
62766695

132



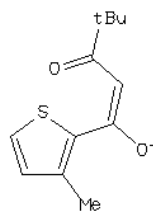
62767398

133

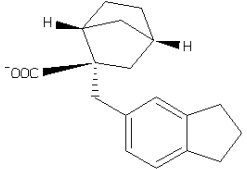
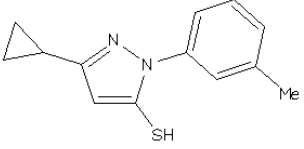
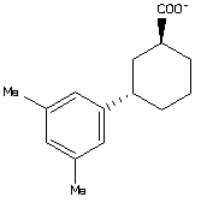
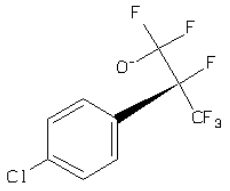
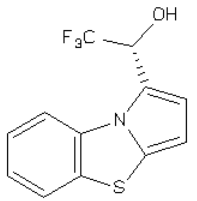
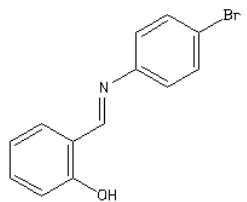
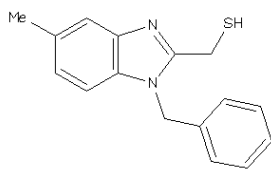


65363987

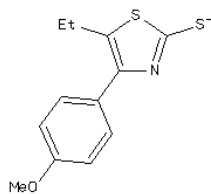
134



70089944

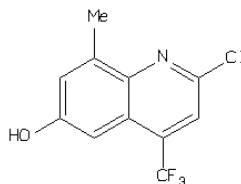
135		70499572
136		71006879
137 (no vendor)		71536153
138		71609844
139 (Available from Sigma Aldrich: 250 USD/25mg)		71781983
140 (Available from Sigma Aldrich: 100 USD/1g)		13406338
141 (no vendor)		74295617

142
(no vendor)



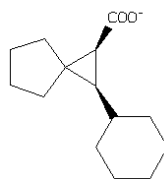
75420767

143
(no vendor)



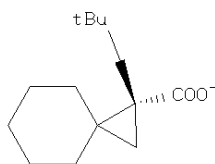
75895622

144
(no vendor)



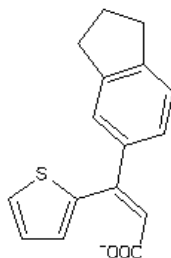
76672500

145
(no vendor)



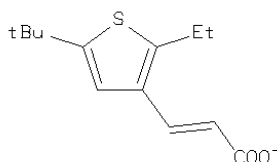
76673892

146
(no vendor)



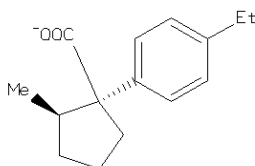
76709587

147
(no vendor)



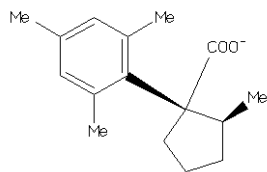
77096210

148
(no vendor)



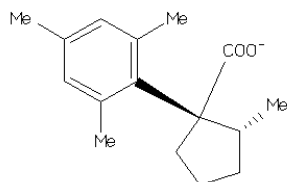
77363550

149
(no vendor)



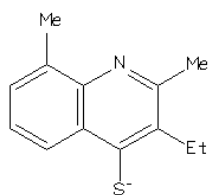
77402526

150
(no vendor)



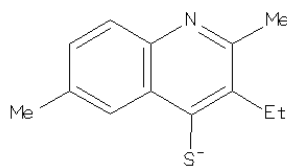
77402532

151



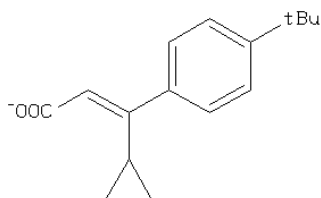
04798082

152



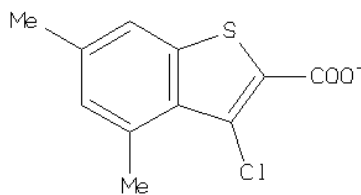
04798083

153
(no vendor)



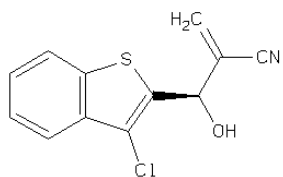
11628540

154



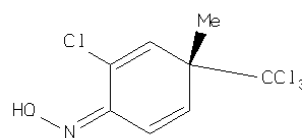
12778417

155



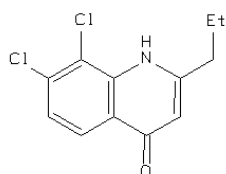
19836268

156



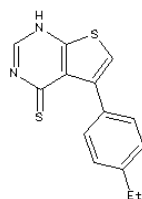
16890089

157



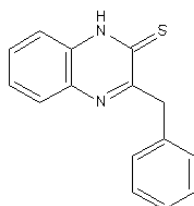
32099927

158



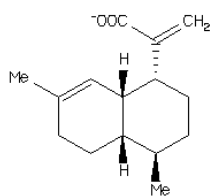
31933493

159



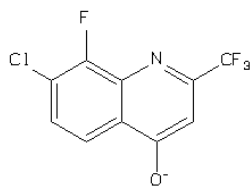
32916891

160



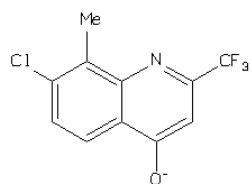
34564537

161



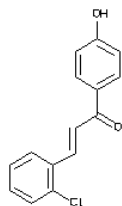
36912416

162



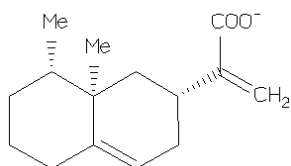
36912540

163



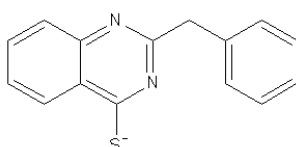
04428581

164



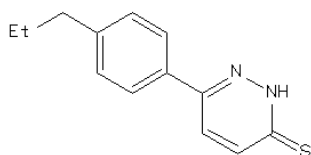
31165788

165



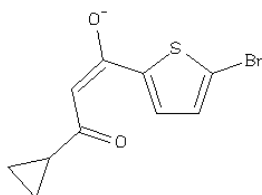
03063698

166



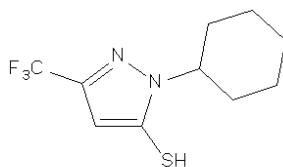
41256497

167



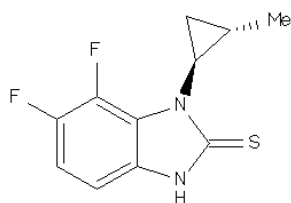
49866614

168



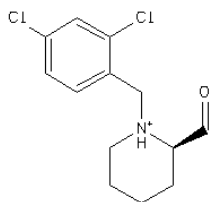
52305697

169



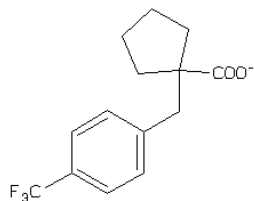
53169402

170



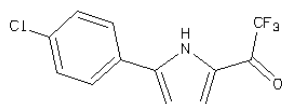
54237822

171



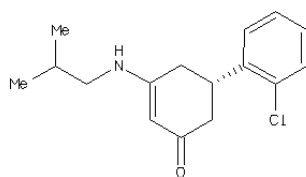
54632593

172



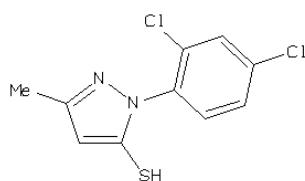
04893003

173



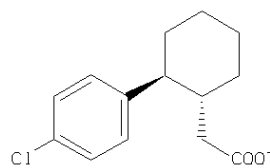
58866428

174



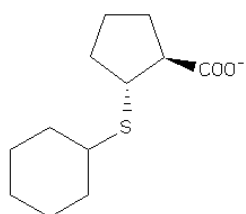
52304993

175



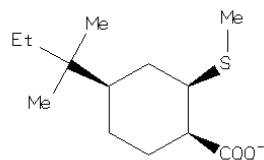
62624754

176



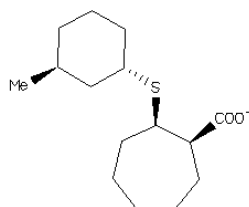
62766306

177



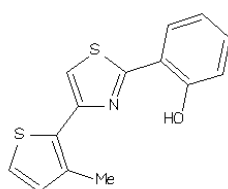
62766694

178



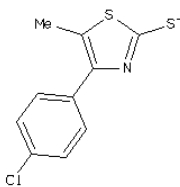
62767409

179



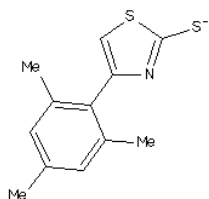
70090150

180



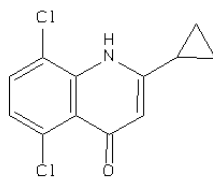
70598214

181



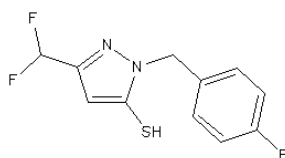
70598286

182

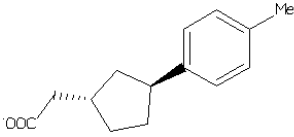
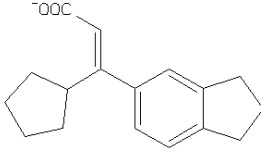
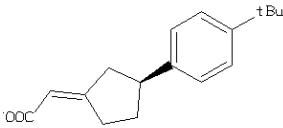
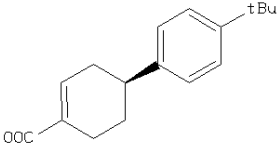
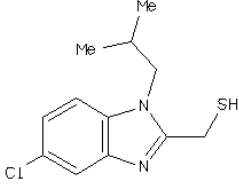
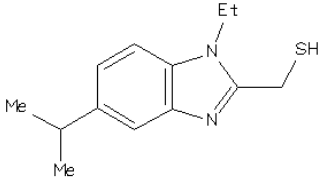
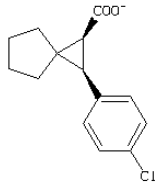


71008597

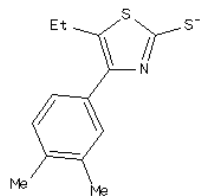
183



71193444

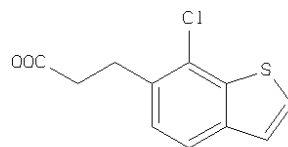
184 (no vendor)		71520565
185 (no vendor)		71577639
186 (no vendor)		71584539
187 (no vendor)		71584541
188 (no vendor)		71744442
189 (no vendor)		74297428
190 (no vendor)		75192882

191
(no vendor)



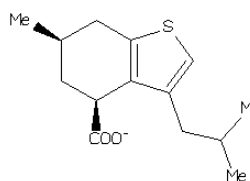
75420753

192
(no vendor)



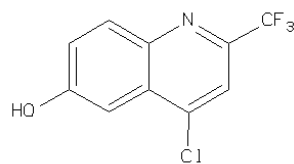
75431837

193
(no vendor)



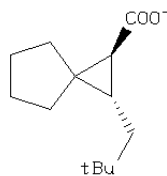
75628658

194
(no vendor)



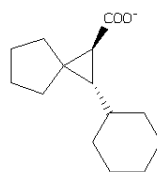
75893709

195
(no vendor)



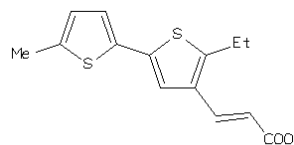
76643068

196
(no vendor)



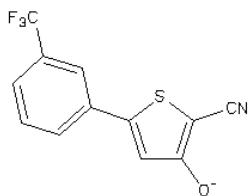
76672501

197
(no vendor)



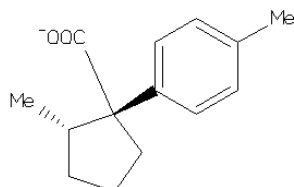
77097989

198
(no vendor)



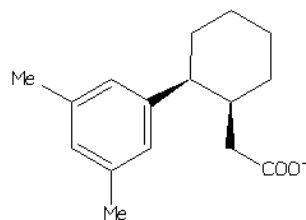
77098336

199



77326379

200
(no vendor)



77402607

References

1. Westermark, P., et al., *Amyloid: toward terminology clarification. Report from the Nomenclature Committee of the International Society of Amyloidosis*. *Amyloid*, 2005. **12**(1): p. 1-4.
2. Chiti, F. and C.M. Dobson, *Protein misfolding, functional amyloid, and human disease*. *Annu Rev Biochem*, 2006. **75**: p. 333-66.
3. Cao, P., A. Abedini, and D.P. Raleigh, *Aggregation of islet amyloid polypeptide: from physical chemistry to cell biology*. *Curr Opin Struct Biol*, 2013. **23**(1): p. 82-9.
4. Opie, E.L., *The Relation Of Diabetes Mellitus to Lesions of the Pancreas. Hyaline Degeneration of the Islands Of Langerhans*. *J Exp Med*, 1901. **5**(5): p. 527-40.
5. Westermark, P., et al., *Amyloid fibrils in human insulinoma and islets of Langerhans of the diabetic cat are derived from a neuropeptide-like protein also present in normal islet cells*. *Proc Natl Acad Sci U S A*, 1987. **84**(11): p. 3881-5.
6. Cooper, G.J., et al., *Purification and characterization of a peptide from amyloid-rich pancreases of type 2 diabetic patients*. *Proc Natl Acad Sci U S A*, 1987. **84**(23): p. 8628-32.
7. Westermark, P., A. Andersson, and G.T. Westermark, *Islet amyloid polypeptide, islet amyloid, and diabetes mellitus*. *Physiol Rev*, 2011. **91**(3): p. 795-826.
8. Westermark, P., et al., *Islet amyloid polypeptide: pinpointing amino acid residues linked to amyloid fibril formation*. *Proc Natl Acad Sci U S A*, 1990. **87**(13): p. 5036-40.
9. Wiltzius, J.J., et al., *Atomic structure of the cross-beta spine of islet amyloid polypeptide (amylin)*. *Protein Sci*, 2008. **17**(9): p. 1467-74.
10. Sanke, T., et al., *An islet amyloid peptide is derived from an 89-amino acid precursor by proteolytic processing*. *J Biol Chem*, 1988. **263**(33): p. 17243-6.
11. Konarkowska, B., et al., *The aggregation potential of human amylin determines its cytotoxicity towards islet beta-cells*. *FEBS J*, 2006. **273**(15): p. 3614-24.
12. Khemtournian, L., et al., *Recent insights in islet amyloid polypeptide-induced membrane disruption and its role in beta-cell death in type 2 diabetes mellitus*. *Exp Diabetes Res*, 2008. **2008**: p. 421287.
13. Cao, P., et al., *Islet amyloid polypeptide toxicity and membrane interactions*. *Proc Natl Acad Sci U S A*, 2013. **110**(48): p. 19279-84.
14. Buchanan, L.E., et al., *Mechanism of IAPP amyloid fibril formation involves an intermediate with a transient beta-sheet*. *Proc Natl Acad Sci U S A*, 2013. **110**(48): p. 19285-90.
15. Mishra, R., et al., *Inhibiting islet amyloid polypeptide fibril formation by the red wine compound resveratrol*. *Chembiochem*, 2009. **10**(3): p. 445-9.
16. Jiang, P., et al., *Resveratrol inhibits the formation of multiple-layered beta-sheet oligomers of the human islet amyloid polypeptide segment 22-27*. *Biophys J*, 2011. **100**(6): p. 1550-8.
17. Cao, P. and D.P. Raleigh, *Analysis of the inhibition and remodeling of islet amyloid polypeptide amyloid fibers by flavanols*. *Biochemistry*, 2012. **51**(13): p. 2670-83.
18. Sumner Makin, O. and L.C. Serpell, *Structural characterisation of islet amyloid polypeptide fibrils*. *J Mol Biol*, 2004. **335**(5): p. 1279-88.
19. Luca, S., et al., *Peptide conformation and supramolecular organization in amylin fibrils: constraints from solid-state NMR*. *Biochemistry*, 2007. **46**(47): p. 13505-22.

20. Tharp, W.G. and I.N. Sarkar, *Origins of amyloid-beta*. BMC Genomics, 2013. **14**: p. 290.
21. Aitken, J.F., et al., *Suppression by polycyclic compounds of the conversion of human amylin into insoluble amyloid*. Biochem J, 2003. **374**(Pt 3): p. 779-84.
22. Noor, H., *Using Small Molecules to Study Amyloid Formation by Islet Amyloid Polypeptide*(Master's thesis).
23. Feng, B.Y., et al., *Small-molecule aggregates inhibit amyloid polymerization*. Nat Chem Biol, 2008. **4**(3): p. 197-9.
24. Krebs, M.R., E.H. Bromley, and A.M. Donald, *The binding of thioflavin-T to amyloid fibrils: localisation and implications*. J Struct Biol, 2005. **149**(1): p. 30-7.
25. Moustakas, D.T., et al., *Development and validation of a modular, extensible docking program: DOCK 5*. J Comput Aided Mol Des, 2006. **20**(10-11): p. 601-19.
26. Abedini, A. and D.P. Raleigh, *Incorporation of pseudoproline derivatives allows the facile synthesis of human IAPP, a highly amyloidogenic and aggregation-prone polypeptide*. Org Lett, 2005. **7**(4): p. 693-6.
27. Abedini, A., G. Singh, and D.P. Raleigh, *Recovery and purification of highly aggregation-prone disulfide-containing peptides: application to islet amyloid polypeptide*. Anal Biochem, 2006. **351**(2): p. 181-6.
28. Khan, M.T., *Novel tyrosinase inhibitors from natural resources - their computational studies*. Curr Med Chem, 2012. **19**(14): p. 2262-72.
29. Supuran, C.T., *Structure-based drug discovery of carbonic anhydrase inhibitors*. J Enzyme Inhib Med Chem, 2012. **27**(6): p. 759-72.
30. Sierotzki, H. and G. Scalliet, *A review of current knowledge of resistance aspects for the next-generation succinate dehydrogenase inhibitor fungicides*. Phytopathology, 2013. **103**(9): p. 880-7.
31. Mohan, V., et al., *Docking: successes and challenges*. Curr Pharm Des, 2005. **11**(3): p. 323-33.
32. Huang, N., B.K. Shoichet, and J.J. Irwin, *Benchmarking sets for molecular docking*. J Med Chem, 2006. **49**(23): p. 6789-801.
33. Verdonk, M.L., et al., *Virtual screening using protein-ligand docking: avoiding artificial enrichment*. J Chem Inf Comput Sci, 2004. **44**(3): p. 793-806.
34. Irwin, J.J. and B.K. Shoichet, *ZINC--a free database of commercially available compounds for virtual screening*. J Chem Inf Model, 2005. **45**(1): p. 177-82.
35. Mysinger, M.M. and B.K. Shoichet, *Rapid context-dependent ligand desolvation in molecular docking*. J Chem Inf Model, 2010. **50**(9): p. 1561-73.
36. Mysinger, M.M., et al., *Directory of useful decoys, enhanced (DUD-E): better ligands and decoys for better benchmarking*. J Med Chem, 2012. **55**(14): p. 6582-94.
37. Vogel, S.M., M.R. Bauer, and F.M. Boeckler, *DEKOIS: demanding evaluation kits for objective in silico screening--a versatile tool for benchmarking docking programs and scoring functions*. J Chem Inf Model, 2011. **51**(10): p. 2650-65.
38. Hudson, S.A., et al., *The thioflavin T fluorescence assay for amyloid fibril detection can be biased by the presence of exogenous compounds*. FEBS J, 2009. **276**(20): p. 5960-72.
39. LaPlante, S.R., et al., *Compound aggregation in drug discovery: implementing a practical NMR assay for medicinal chemists*. J Med Chem, 2013. **56**(12): p. 5142-50.